POLITECNICO DI TORINO
Repository ISTITUZIONALE

A review on near net shape hot isostatic pressing of metallic materials: For industrial applications

Original
A review on near net shape hot isostatic pressing of metallic materials: For industrial applications / Anwar, J., Bassini, E., Fino, P., Lombardi, M., Bondioli, F., Aristizabal, M., Iturriza, I.Z., Biamino, S., Ugues, D.. - In: JOURNAL OF MATERIALS RESEARCH AND TECHNOLOGY. - ISSN 2238-7854. - 42:(2026), pp. 3663-3684. [10.1016/j.jmrt.2026.03.210]

Availability:
This version is available at: 11583/3009774 since: 2026-04-10T09:14:36Z

Publisher:
Elsevier

Published
DOI:10.1016/j.jmrt.2026.03.210

Terms of use:

This article is made available under terms and conditions as specified in the corresponding bibliographic description in the repository

Publisher copyright

(Article begins on next page)

18 November 2026

Journal of Materials Research and Technology 42 (2026) 3663–3684

Contents lists available at ScienceDirect

Journal of Materials Research and Technology

journal homepage: www.elsevier.com/locate/jmrt

A review on near net shape hot isostatic pressing of metallic materials: For industrial applications

Jehanzaib Anwar [a], Emilio Bassini [a,*], Paolo Fino [a], Mariangela Lombardi [a], Federica Bondioli [a], Miren Aristizabal [b], Inigo Zubillaga Iturriza [b], Sara Biamino [a], Daniele Ugues [a]

[a] Department of Applied Science and Technologies (DISAT) Politecnico di Torino, Corso Duca Degli Abruzzi 24, 10129, Torino (To), Italy
[b] CEIT-Basque Research and Technology Alliance (BRTA), Manuel Lardizabal 15, 20018 Donostia, San Sebastián, Spain

ARTICLE INFO

Keywords:
Hot isostatic pressing
Near net shape
Powder metallurgy
Metallic materials

ABSTRACT

The utilization of metallic materials with superior mechanical properties is growing in high-end applications. However, the fabricability of these materials has some significant challenges. To address these challenges, near-net shape (NNS) hot isostatic pressing (HIP) emerged as an effective technique, providing a leaner and more efficient single-step method to manufacture near-net shapes from powders. This article reviews the existing literature on NNS-HIP of metallic materials, covering the entire process from design to final inspection, and explores strategies for overcoming current challenges. The primary focus is to illustrate its industrial applicability while identifying factors that hinder its broader adoption. The findings suggest that continued research and systematic optimization of each step of NNS-HIP are required to achieve a compound effect, making the overall process more cost-effective and enhancing its industrial applicability.

1. Introduction

Due to technological advancements, demand for materials with superior mechanical properties is increasing to cater to high-end applications. However, with the improved mechanical properties, the ease of fabricability becomes a challenging task. For example, superalloys and refractory metals are ideal for aerospace and other high-temperature applications due to their outstanding properties. However, machining them can be a cumbersome task. Furthermore, conventional techniques like forging, casting, etc., can also induce cracks and segregation in highly alloyed metals, which are unacceptable for critical applications [1]. Moreover, uneven grain size and precipitation are the drawbacks of conventional methods and contribute to the variability in material properties [2]. Also, additional welding is required in traditional techniques, adding weight to the final part while introducing distortion and stress to the material.

To address these challenges, the powder metallurgy (PM) route can be adapted to manufacture difficult-to-fabricate parts via conventional methods. Currently, the leaner and more efficient single-step method to manufacture near-net shapes (NNS) from powders using hot isostatic pressing (HIP), known as NNS-HIP, is used to manufacture the components. This technique takes less time compared to traditional powder manufacturing routes. Moreover, it also has a low buy-to-fly ratio compared to conventional machining processes. Furthermore, uniform properties, less welding resulting in less weight, easy inspectability, complex design, and defect-free dense structure are also characteristics of components fabricated using the HIP technique. However, NNS-HIP also has some limitations, including high cost, possible higher oxygen content, especially in the finer powder, and a limited number of parts per cycle [3,4].

Previously, few researchers have reviewed HIP, but initially, the reviews were more focused on the equipment and its functions [5]. Later, H.V. Atkinson and S. Davies [4] reviewed HIP, giving a comprehensive overview of the HIP, including the basis of sintering, and modeling techniques were also discussed in more detail. Similarly, M. H. Bocanegra Bernal [6] also reviews HIP, focusing more on ceramics as time demands, since ceramics were the first materials produced using HIP technology, and research was initially more focused on ceramic materials. Currently, the industry is demanding metallic and composite parts for more stringent applications as discussed. Therefore, more recently, Javadzadeh K et al. [7] also evaluated the topic comprehensively, focusing on the microstructure and fatigue behavior of

* Corresponding author. Politecnico di Torino – Dipartimento di Scienza dei Materiali e Ingegneria Chimica Torino, Italy.
E-mail address: emilio.bassini@polito.it (E. Bassini).

https://doi.org/10.1016/j.jmrt.2026.03.210
Received 27 October 2025; Received in revised form 19 January 2026; Accepted 25 March 2026
Available online 6 April 2026
2238-7854/© 2026 Published by Elsevier B.V. This is an open access article under the CC BY-NC-ND license (http://creativecommons.org/licenses/by-nc-nd/4.0/).

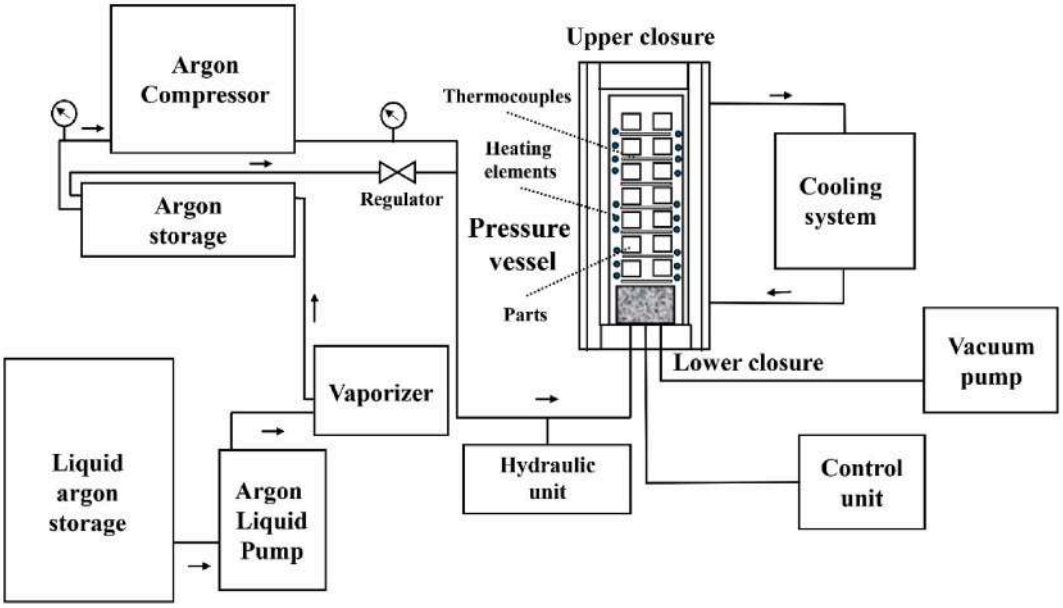


Fig. 1. Schematic diagram of HIP equipment.

PM-HIPped nickel superalloys and tool steel specifically. Cui et al. [8] also reviewed the topic, focusing specifically on powder HIP of titanium alloys and the role of numerical simulation. Thus, a comprehensive review of the NNS-HIPping for metallic materials is needed for recent advancements in this field and its industrial applications.

In this article, HIP is examined with more focus on the recent advancements in NNS and its practical use. The main objective of this research is to realize the importance and industrial applicability of HIP for metals and what further can be done to increase the market penetration of this technology. In the current study, the HIPping process, from powder preparation to inspection, is comprehensively reviewed. Section 2 discusses the background and explains the process of HIP. Section 3 examines the powder processes used for powder preparation and the properties of powders. In section 4, the most important economic parameter, the canning of powder, is discussed. Section 5 explores a few high-demand metals relevant to the HIP process. Section 6 sheds some light on the modeling techniques used for the prediction of the final shape of the part. Lastly, the concluding section explains the latest industrial developments in the field of NNS-HIP and concludes the review.

2. Background and process

The lab scale HIP was initially developed by ABB in Sweden in 1950 and Battelle Memorial Institute in the US in 1960. Silicon nitride and silicon carbide were the first commercially produced high-performing ceramics through HIP. Before that, oxide ceramics such as lead zirconate titanate (PZT), partially stabilized zirconia (PSZ), etc., were made successfully using HIP technology [6]. Fig. 1 schematically shows the standard HIP equipment diagram, including the pressure system, heating system, gas storage, cooling unit, and control units, providing a visual overview of the main operational components. HIP is a process widely used to improve the density and mechanical properties of materials. It involves subjecting the material to a combination of high temperature (up to 2000 °C) and isostatic pressure (up to 300 MPa) by the action of gas (argon, nitrogen, helium), facilitating the transfer of isostatic high pressure to the part, eliminating internal voids and defects. This high-temperature, high-pressure environment is also effective for densifying powders to final components. Usually, HIPping is performed at a temperature approximately 20% below the solidus line while simultaneously applying isostatic pressure, depending on the type of material. The HIP cycle typically consists of pressure vessel evacuation, pressurization, heating to the target temperature, isothermal holding, and controlled cooling. For achieving the high temperature in the HIP chamber, three types of heating elements can be used based on the temperature required in the chamber: Kanthel, molybdenum, and graphite for up to 1000 °C, 1450 °C, and 2000 °C or above. Kanthel heating elements can be loaded and unloaded at higher temperatures. However, for graphite and molybdenum, cold loading and unloading are needed; otherwise, it can cause oxidation. This gives an advantage to kanthel in terms of saving time over other heating elements [6]. Since HIPping is done at high pressures and temperatures, safety considerations must be addressed both prior to and throughout its operation. Initially, many researchers raised concerns about the safety of its equipment, but later, this was addressed by introducing a pre-stressed wire coiled around the chamber [9]. Furthermore, multiple safety checks with sensors and alarms have also been incorporated into the HIP equipment to increase the safety factors.

The HIPping process can be used for manufacturing NNS, post-processing treatment [10], rejuvenation treatment [11], and to produce joints of similar as well as dissimilar metals by diffusion bonding [12]. No significant shape change is observed after the HIPping process in post-processing treatment due to the already high density of the component, leaving minimal porosity to be compacted. However, for NNS-HIPping, the density in the capsule is only about 60-70%. When high temperature and pressure are applied, densification begins with particle rearrangement, eventually leading to a dense structure where isolated pores collapse and near-theoretical density is achieved. Due to which shape change of approximately 30% is usually observed. Therefore, the necessary allowance must be kept during the densification of NNS parts. In some cases, machining is required after NNS produces parts. However, the machining required after NNS-HIPping is 3-4 times less than that needed for parts fabricated using conventional methods, limited to finishing operations such as dimensional adjustments, surface finishing, threading, slotting, assembly fitment, etc. Owing to the near-theoretical density and low defects in the HIPped parts, it was observed that the failure rate of HIPped parts is significantly lower compared to non-HIPped parts. As reported by Ruys et al. [13] the

failure rate of HIPped alumina prosthetic hip joints is about 0.004% compared to conventionally sintered components, which was up to 10%.

2.1. Near net shape hot isostatic pressing

In the context of the fabrication of NNS via hot isostatic pressing equipment, the process begins with designing the container known as a "capsule", in which powder is filled for consolidation. However, filling powder is a complicated process during which multiple factors must be considered to achieve a minimum density of approx. 65% before pressing [14]. An out-gassing process must be carried out to remove the entrapped gases after filling the powder to avoid defects and improve the reproducibility of parts. It has been observed that simple evacuation is not enough with the help of a vacuum pump for complete degassing, as the powder particles can have microscopic porosity and irregular surfaces where gases can be trapped. Additionally, powders have different rheological properties, causing issues in the settlement of the powder for the achievement of uniform density in the capsule, making the filling process further complicated. To overcome these issues, the filling is performed at elevated temperatures, which helps release the entrapped gases. As the temperature increases, the viscosity and energy barrier for the desorption of gases decrease, resulting in the easy removal of gases from the powder using the vacuum pump. Moreover, vibration is also introduced during the filling stage to improve powder packing. Without vibration, powders may form loose or uneven layers, resulting in non-uniform pressure distribution during HIPping. Vibration helps to rearrange the particles, reduce voids, and increase the packing density, which ensures more uniform consolidation and minimizes the risk of defects in the final product. After filling the capsule, welding is performed to seal the capsule, preventing the penetration of gases into the system. The sealed capsule is then placed in the HIP chamber to apply high temperature and pressure, resulting in the densification of the powder, eliminating voids, and achieving near-theoretical-density material. After HIPping, the capsule is removed, and the component undergoes finishing and inspection before use.

NNS-HIP has six main operations as illustrated in Fig. 2: designing, filling, welding, HIPping, removing, and finishing [15].

During the HIPping cycle, the powder goes through various stages.

- Stage 0: At the beginning, only adhesion bonding is present between the particles. After pressure is applied, the particle rearrangement and instantaneous plastic deformation starts.
- Stage 1: This stage starts when the temperature is applied to the capsule. Diffusion starts between the particles (both grain boundary and lattice), and necks begin to appear between them. With time, the necks grow, and the open porosity transforms into closed porosity.
- Stage 2: This stage begins with closed porosity. Further increase in temperature and pressure reduces the size of the closed porosity by allowing the gas to dissolve into the metal and plastic deformation by creep [16].

Mostly argon is used as a pressurizing gas in the HIP equipment. However, gases other than argon can also be used for HIPping. Helium offers multiple advantages over argon as it has lower density and greater thermal conductivity, resulting in uniform temperature distribution on the samples, but is more expensive. Furthermore, nitrogen gas is used, especially in the case of HIPping of silicon nitride, preventing the deterioration of nitrides [17]. NNS-HIPping can produce much larger parts, but in a limited quantity compared to other PM methods [3]. The key advantage of NNS-HIP over other PM processes is its ability to fabricate large and complicated parts in a lean, single-step process. Therefore, to further enhance its competitiveness and industrial acceptability, the development of larger HIP equipment is required to make the process more economical. As of now, the largest HIP equipment at MTC Japan can produce parts up to 28 tons. The equipment has a diameter of 2050 mm and a height of 4050 mm.

2.1.1. Comparison of NNS-HIP with other technologies

When compared to conventional manufacturing technologies, NNS-HIP can offer the following advantages in comparison.

- Fine and homogeneous isotropic microstructure.
- Reduction of the number of welds.
- Easy inspection.
- Fabrication of complex shapes with a single-step process.
- Reduction of machining costs.
- Cost benefits, especially for expensive materials, due to low buy-to-fly ratio.
- Producing a small series of large and complex shapes.

According to an EPMA report in 2016 [18,19] % of the market share in Europe is still with sinter products, and only 6% of parts are being manufactured using HIP, as shown in Fig. 3. But in North America, press-sinter products have shrunk by 20%, showing the shifting trends towards emerging PM techniques i.e., MIM, HIPping technology etc. Moreover, the global isostatic pressing market reached a value of USD 7.6 billion in 2024, with an estimated compound annual growth rate (CAGR) of 5.45% till 2029, anticipated to drive the market size to USD 9.9 billion [20].

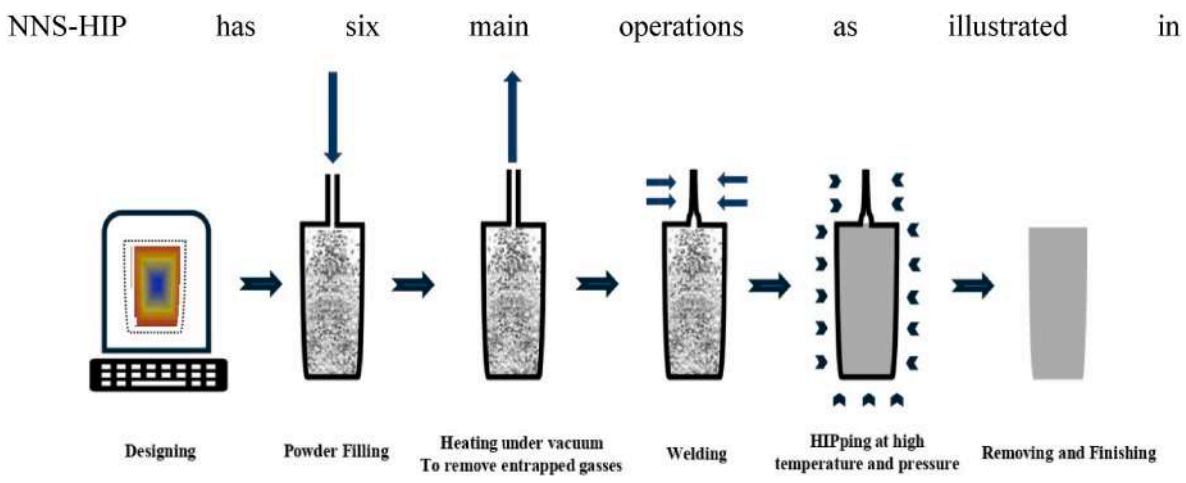


Fig. 2. Schematic depiction of NNS-HIP Process.

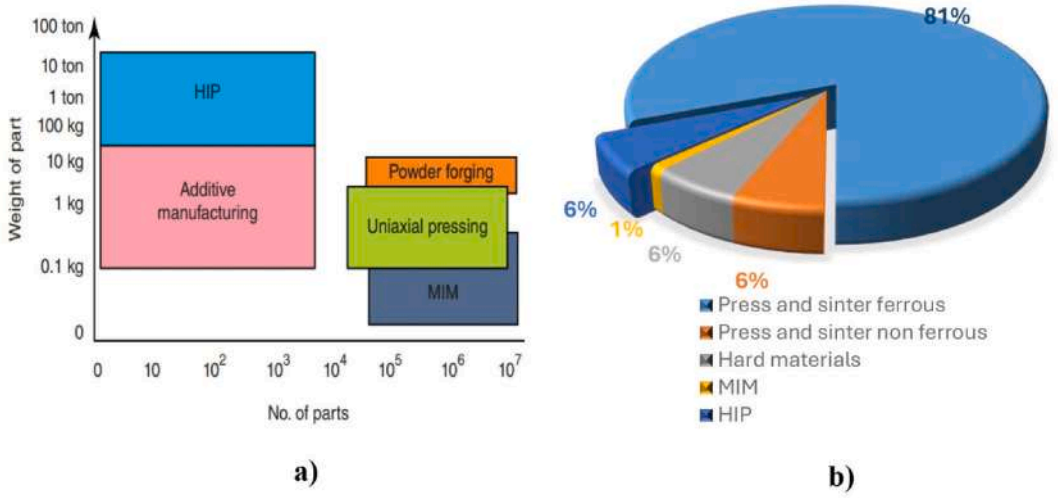


Fig. 3. (a) Positioning of PM HIP technology versus other PM technologies. (b) European PM production by tonnage (EPMA) in 2016 [18].

Notable example of this renewed interest for PM can be seen in the nuclear field where PM (HIP) combined with electron beam welding (EBW) for small modular reactor fabrication will cut the cost by 40%, 60% of production time, and 70% of welding time. It has also been reported that the cost is 20-30% less in the case of expensive metals if the PM-HIP route is adopted instead of conventional methods due to the low by-to-fly ratio, less welding, and easy ultrasonic testing (UT) inspection [18]. Furthermore, in UT inspection, the first few millimeters are known as dead areas or near-surface areas, which are considered a limitation. But in the case of NNS, this dead area can be covered by tooling, and 100% inspection of the NNS part can be performed. Moreover, fine-grain size also results in less distortion and easy inspection, as Krautkrämer and Krautkrämer [21] explained that the large grains create stronger and more irregular scattering because the coarse grain sizes are comparable to the wavelength of the ultrasonic waves used for inspection, resulting in more intense reflection, diffraction, and mode conversion. Another unique advantage of NNS using HIP is that complex shapes can be achieved, like casting. Still, maintaining properties comparable to the wrought alloys, or in some cases, the effective properties are greater than the wrought alloys due to less scatter as the design is done with the lowest values.

HIP has multiple advantages, but it also has some future challenges related to its size, shape, and materials. These issues will be addressed with improvements in research and technology. For example, powders are used as the primary unit for manufacturing NNS. Consequently, the fundamental chemical difference between the HIPped and forged parts lies in oxygen content. Due to the presence of oxygen and higher surface energy, oxides and carbides are formed on the powders' surface, known as prior particle boundary (PPBs), degrading the HIPped part's mechanical properties [22]. Consequently, continued advancements in powder production, handling, and HIP processing strategies are required to minimize such defects and improve overall material quality.

Despite some limitations related to the HIPping process and equipment, ongoing research and development efforts effectively addressing and overcoming the existing bottlenecks. Recent developments in HIPping technology have made it more compatible with industrial needs. HIP has become large. Manufacturers have developed and adopted fast cooling & recently, quenching technologies in HIP equipment, to increase the cooling rate to 3000 °C/min [23]. With the help of these techniques, Material can be simultaneously heat-treated in the HIP and reduce the cycle time to 70% [18]. Moreover, multiple techniques, including heat and mechanical treatments of powder and HIPped parts, discussed in the next section, are effective in improving the quality. In addition, choosing the optimum powder size and atomization process also leads to minimizing the effect of deteriorating oxide layers [24].

2.1.2. *Uniform densification challenges in large NNS-HIP components*

Besides PPBs, uniform densification is also one of the most critical technological challenges in the broader industrial adoption of NNS-HIP, particularly for large and geometrically complex components. While HIP is often idealized as a near-net shape isostatic process, practical deviations from uniform densification arise from coupled thermo-mechanical, material, and geometric effects that become more significant as the component size increases.

2.1.2.1. Thermo-mechanical origins of non-uniform densification. In large HIPped components, it is very difficult to maintain perfectly homogeneous temperature and pressure gradients throughout the powder capsule. Several studies have demonstrated that thermal gradients, driven by differences in thermal conductivity between loose powder, partially consolidated powder, capsule material, and pressurizing gas, lead to variations in densification kinetics. For example, Essa et al. [25] showed that during the consolidation of IN718 powder, the powder core experiences delayed heating relative to near-surface regions due to lower effective thermal conductivity, resulting in radial density gradients during early HIP stages, as will be discussed in detail in the modeling section. Similarly, Yuan et al. [26] demonstrated that HIP processing of cylindrical Ti–6Al–4V powder components leads to pronounced anisotropic shrinkage, with radial contraction significantly exceeding axial shrinkage, despite nominally isostatic pressure conditions, mainly due to the capsule constraint and non-uniform stress.

2.1.2.2. Role of initial powder packing and filling heterogeneity. Uniform densification is fundamentally constrained by the initial relative density distribution inside the capsule. For large components, achieving homogeneous powder packing is increasingly difficult due to gravitational segregation, particle-size stratification, and limited powder flowability. Broeckmann [16] emphasized that variations in initial relative density can translate into macroscopic shape distortions and density non-uniformity after HIP, particularly when capsule deformation is constrained. This variation can be reduced by inducing vibration during filling, as already discussed, but as the size of the capsules increases, the effect is exacerbated as the vibration energy during filling attenuates with distance from the vibration source. Experimental validation was provided by Van Nguyen et al. [27], who showed that inhomogeneous initial powder density distributions cause anisotropic shrinkage and

distortion during PM-HIP, with low-density regions shrinking more and inducing non-uniform shape changes, especially in large components.

2.1.2.3. Capsule-powder interaction and directed deformation effects. In large-scale NNS-HIP, the capsule itself becomes an active mechanical participant in the densification process. Therefore, variations in capsule thickness, weldments, and material can introduce deviatoric stresses, negating the assumption of uniform loading.

To mitigate the anisotropic shrinkages, different strategies are discussed in more detail in Section 4, in which glass capsules are used to promote isotropic shrinkages [28]. Moreover, locally thickened walls or reinforcing features are used to compensate for expected shrinkage gradients [29].

2.1.2.4. Industrial-scale evidence from large hip components. Industrial case studies further confirm that uniform densification is a non-trivial challenge at scale.

- Subsea manifolds and valve bodies manufactured via NNS-HIP [30] exhibited density gradients unless powder filling, capsule design, and HIP cycles were carefully optimized.
- Nuclear pressure-boundary components produced by PM-HIP in combination with electron beam welding have been identified as promising routes for advanced reactor systems, where careful optimization of HIP parameters is essential to achieve full densification and reliable structural integrity [18].
- Giga-HIP systems with working diameters exceeding 2 m that could handle temperatures of 1200 °C, pressures of 118 Mpa, and loading weights of up to 28 tons. This demonstrates the feasibility of HIP at an unprecedented industrial scale. However, as discussed above with examples, scale-up increases susceptibility to thermal gradients and non-uniform densification, necessitating careful thermal management and process optimization to ensure uniform density in large components [31].

2.1.2.5. Modeling-driven mitigation strategies. Advanced modeling has become indispensable for addressing uniform densification in large components. Multiscale approaches integrating powder-scale constitutive behavior with component-scale finite element method (FEM) have shown strong predictive capability. Most notably, Elguezabal et al. [32] achieved densification and shape predictions with errors below 0.2% for a 1500-mm-long Astroloy component by coupling mesoscopic densification laws with macroscopic viscoplastic models. This work clearly demonstrates that uniform densification in large NNS-HIP components is achievable only through integrated process–structure–modeling approaches, rather than empirical parameter selection.

These challenges and mitigation strategies provide the foundation for the detailed discussions on capsule design (Section 4) and numerical modeling approaches (Section 6). Having established the fundamentals of the HIP and NNS-HIP processes, the following section focuses on powder production routes and characteristics, which directly govern densification behavior and defect formation during HIP.

3. Powders

Mostly, NNS parts produced from HIP technology are used in high-end applications. Therefore, their properties, including mechanical, thermal, physical, and microstructure, are of high importance. The most important role in achieving these outcomes lies in the powders used, as the powders serve as the basic building block of material for NNS-HIP, and their properties directly influence the quality of the product. Therefore, the discussion of powders for NNS-HIP is crucial for deeper research and exploration of its role in shaping the properties of the final part. However, one of the primary challenges to producing sound-quality final parts using NNS-HIP is the availability of high-quality and low-cost powders.

3.1. Production of metal powders

Various processes can produce powders [33] with distinct characteristics as shown in Fig. 4.

The powders are selected based on the material and the intended application. Because powders produced from different processes differ based on particle size distribution (PSD), morphology, purity, cost and composition. Among the following, the most used powders in the industry for NNS-HIPping are produced from the atomization processes due to their capability of producing a wide range of particle sizes, depending on their sub-processes and parameters, as shown in Fig. 5. If further classified based on the usage, gas atomization (GA) takes the lead. Gas-atomized powders have poor compressibility but excellent purity. Furthermore, due to narrow PSD, GA produces a high yield. In addition, the compressibility can be improved by the addition of carefully selected lubricating agents [34]. Generally, refractory metal powders are produced by their chemical precursors [35]. However, a few researchers have used multiple powder production methods for

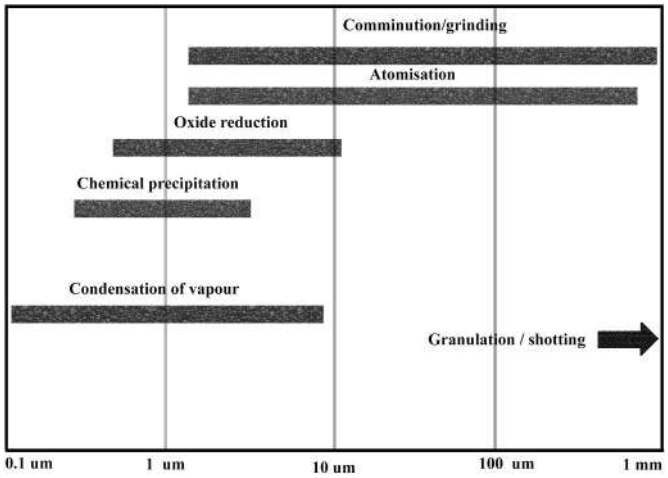


Fig. 5. Approximate powder sizes, produced by different techniques [42].

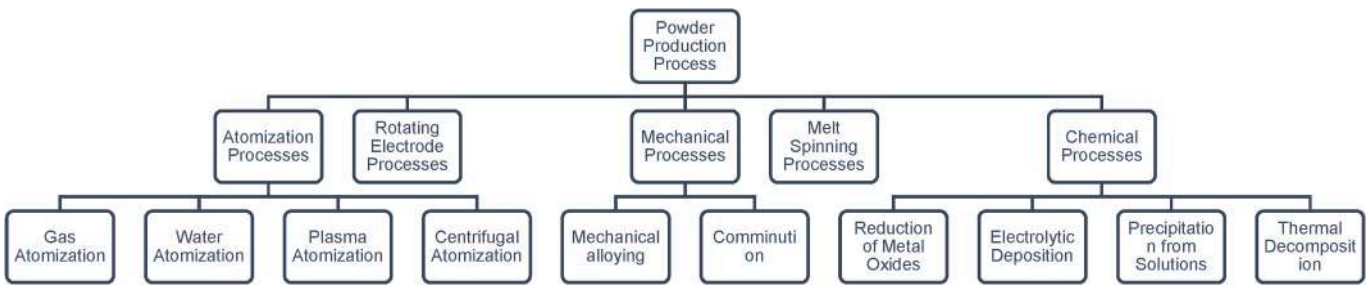


Fig. 4. Metallic powder production processes.

refractory metals. For example, rhenium can be produced using the plasma rotating electrode process (PREP), rotating electrode process (REP), gas atomization rotating electrode process (GA REP), and plasma atomization (PA). However, it was observed that the PA process is the only suitable method for the production of desired particle sizes ranging from 17 to 54 μm and acceptable yield to justify the cost [36]. Plasma atomization (PA) can produce high-purity and fine particles. However, high process costs, including feedstock, make the process less economical [37]. Furthermore, powders produced from the water-atomization (WA) process are favored due to their superior compressibility, green strength, and lower cost. However, surface oxidation in water-atomized powders presents a drawback. Also, if comparable properties are being observed from different types of powders, then water-atomized powders are used due to their cost-effectiveness [38].

Most powder production methods result in wider PSD powders, after which sieving and classification are required. Due to this low yield of fine distribution of size, the expense of the powder further increases, making the complete process expensive. Therefore, more efforts in the research are required to improve the yield of finer PSD directly, reducing the need for classification and ultimately driving down production costs. For instance, advancements in close-coupled atomization systems and optimized gas flow mechanisms aim to produce finer PSD at higher yields, improving cost-efficiency and scalability [39]. However, it is pertinent to mention that NNS parts using HIP can be produced using a wider range of particle sizes compared to other manufacturing techniques, making the process more viable for industrial applications, as shown in Fig. 6 [40]. Furthermore, to produce smaller particles, more energy is required, i.e., faster gas flow [41]. Therefore, using a wider range or coarser powder will reduce the cost of the process, enabling cheaper powder for use in NNS-HIP than other manufacturing techniques. Thus, the most suitable metal powders for HIP are produced by gas atomization, with their spherical shape and particle size distribution (PSD), resulting in high filling density and excellent reproducibility of the HIPped components. Furthermore, a wide range of metallic powders, including refractory metals, with suitable yield and particle size, can be produced using gas atomization [36].

3.2. Influence of powder characteristics on NNS-HIP

The intrinsic properties of powders used in NNS-HIP manufacturing have a direct and significant impact on the final component. This strong correlation directed the research toward the mechanical and chemical properties of the powder. One of the most important properties that needs to be considered while using powder for NNS is the presence of oxides and precipitates on the surface of the powder. These PPBs are microstructural features that form on the surface of the powder during its production and handling. On these boundaries, oxides, precipitates, and impurities accumulate, forming a layer hindering the interaction between the powder particles during densification, leading to incomplete consolidation as shown in Fig. 7. Additionally, hard particles with poor bonding and shapes act as stress concentration points, promoting the initiation of cracks, significantly impacting properties like high-temperature ductility, fatigue life, and stress rupture strength. Therefore, the NNS-HIP process needs to be optimized to avoid PPBs.

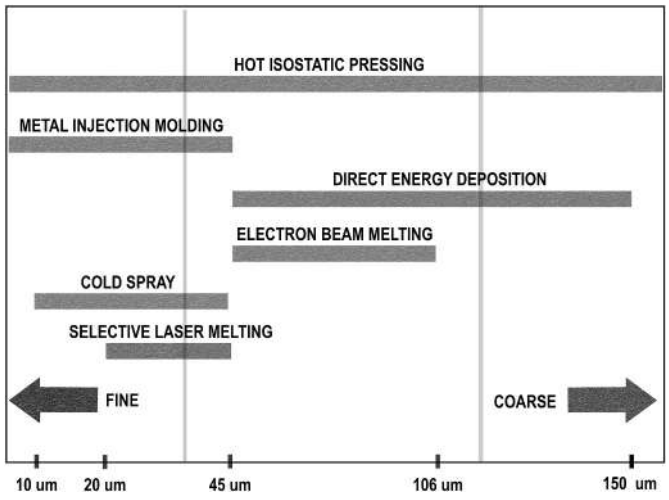


Fig. 6. Particle size distribution of spherical titanium powder for different applications [40,43–45].

In recent years, the surface nature and properties of metal powders have been extensively and systematically investigated using advanced surface-sensitive and microstructural characterization approaches reported in the literature, including, among others, X-ray photoelectron spectroscopy (XPS) (powder surface composition), X ray diffraction (XRD) (Particle phases), Energy dispersive spectroscopy (particle composition), Laser diffraction (Particle size distribution), Helium pycnometry (Density of particle) and high-resolution SEM/TEM (Particle morphology and microstructure) [46–48]. Studies on stainless steels, titanium alloys, and nickel-based superalloys consistently show that powder particles are covered by nanometer-scale oxide films, whose thickness, chemistry, and continuity strongly depend on the atomization route, particle size, alloy composition, and post-atomization exposure or storage conditions. For example, Fleischmann et al. [24] demonstrated that decreasing particle size in gas-atomized 316L stainless steel powders leads to increased oxygen content and thicker oxide layers, as revealed and analyzed by XPS, Raman spectroscopy, and TEM/STEM-EELS analyses. Using XPS-based surface and depth profiling combined with electron microscopy and mechanical testing, Guo et al. [49] and Zhang et al. [50] further showed that oxide growth during powder storage intensifies PPB severity and results in a marked reduction in ductility in HIPped Ti- and Ni-based alloys. Collectively, these studies establish a clear mechanistic link between surface oxides formed during powder production, handling, and storage and the chemical origin of PPBs after HIP consolidation, directly connecting powder surface chemistry to PPB-related microstructural defects and mechanical performance degradation.

Based on these findings, several key parameters governing PPB formation and evolution can be identified, including HIPping temperature, powder storage time, post-processing treatments, and particle size distribution. The individual effects of these parameters are discussed in detail in the following subsections.

3.2.1. Effect of temperature

C. L. Qiu et al. [51] studied powder morphology and the effect of heat treatment on the PPBs in nickel-based superalloy powder RR1000, with a particular focus on Hafnium (Hf). It was observed that, after heat treatment of powder above the solvus temperature, Hf diffuses towards the surface, resulting in the formation of oxides at the PPBs. However, after HIPping, the number of PPBs reduces due to the increase in grain size and migration of the Hf oxides in the grains. This effect was more predominant when HIPping was performed above solvus temperature than below because the dissolution of gamma prime particles further promoted grain boundaries to move across PPBs. Furthermore, it was also noted that sub-solvus HIPping temperature increases yield strength but decreases ductility and ultimate tensile strength (UTS) at elevated temperatures i.e., 700 °C due to the presence of PPBs, promoting interparticle fracture as shown in Fig. 8. Similarly, another study by Liming Tan et al. [52] also observed the reduction in PPBs in nickel-based superalloy FGH96 with the super-solvus temperature during HIPping, due to the facilitation of the grain boundary migration with the dissolution of gamma prime.

3.2.2. Effect of storage time

In addition to the temperature, duration, and storage conditions, also play a key role in the morphology of PPBs on the powders, which in turn

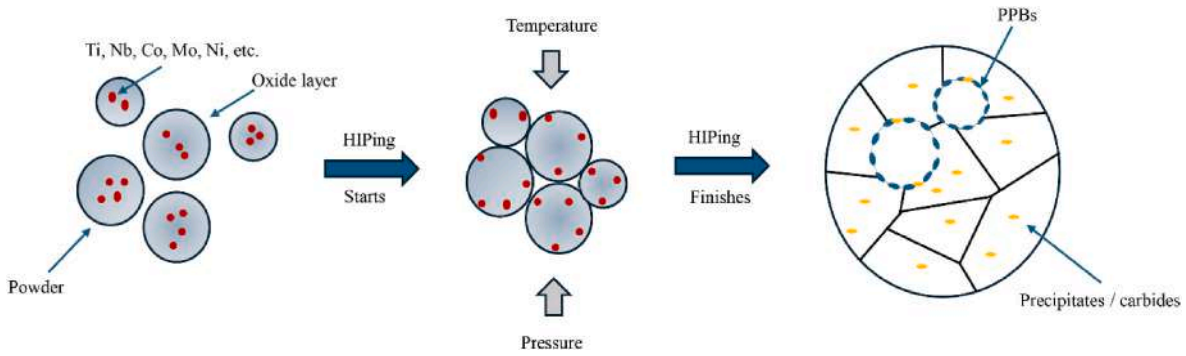


Fig. 7. Schematic diagram for the formation of PPBs during HIP.

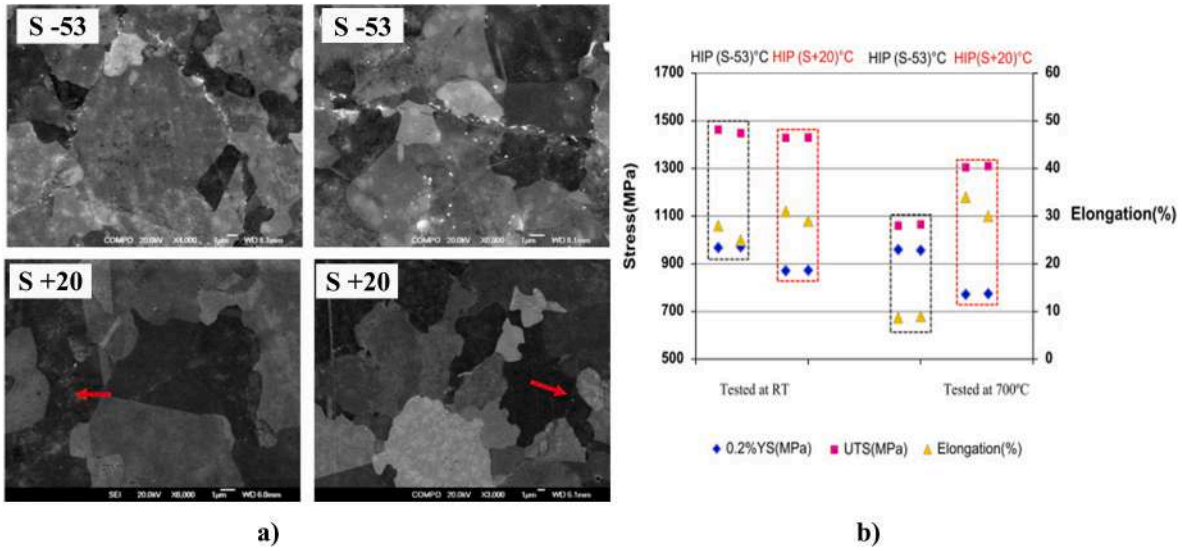


Fig. 8. a) Back-scattered SEM micrographs of HIPped samples at sub (S-53) and super solvus temperatures (S+20). b) Mechanical properties measured at room and elevated temperatures [51].

determines the final properties of the product. Guo, R. et al. [49] investigated the effect of the powder surface state of Ti55 alloy on the mechanical properties of the final product. In their study, powders were kept in a vacuum, and their mechanical properties were studied after 1, 6, and 12 months (PI, PII & PIII). Findings revealed that the samples 1 & 6 months show the same oxide layer formation of 25 & 27 nm, respectively. However, a significant increase in oxide thickness was observed in the third sample of approx. 60 nm estimated through via XPS sputtering using the following numerical formula:

$$d = v_o t_d \quad (1)$$

Where, d is the thickness of the oxide layer (nm), v_o is the sputter rate (nm/s) and t_d is the sputtering time (s) required to reduce the oxygen signal intensity by 50%. This increase in oxide thickness indicate the threshold value for the storage duration after which the oxide layer increases significantly. Furthermore, the mechanical properties were also measured, and it was observed that the properties of 1-month stored powder are comparable to the wrought alloys. However, with increased powder storage time, strength increased and elongation decreased. The decrease in mechanical properties is attributed to the non-breaking oxide layer during HIPping, which forms a lamellar structure and weak bonding areas as depicted in Fig. 9.

Therefore, it can be concluded that 6 months is the shelf time for the storage of titanium powder to achieve the desirable properties. Recently, Zhang et al. [50] also studied the effect of storage conditions on the powder and final part produced. The results indicate the formation of severe PPBs, which leads to the deteriorating properties of the final HIPped part.

3.2.3. *Effect of post-processing treatments*

As already discussed, PPBs in metal powder have a detrimental effect on the mechanical properties of the final materials due to the formation of oxides and carbides. Therefore, reducing the amount of oxides and carbides at PPBs is essential for the improvement of the performance of HIPped components. One of the effective techniques Kuo et al. [53] used at the powder production stage is thermal plasma droplet refining (PDR) to reduce PPBs from the powder surface. Three different samples were prepared, and the effect of PPB reduction was studied. (1) PDR-treated powder sample with reduced PPBs, (2) untreated as HIPped sample, and (3) heat-treated sample containing intermetallic and carbides. The study found that the ductility in PDR samples was improved due to fewer brittle precipitates; however, untreated powders containing PPB exhibited higher tensile strength but poorer ductility due to continuous precipitates acting as the crack initiation points. Furthermore, Heat-treated samples showed severe reduction in ductility, especially at high temperatures, due to the introduction of additional intermetallic phases, needle-like δ phases, and carbides, which further embrittled the material. During material consolidation and subsequent thermo-mechanical processing, mechanical and thermomechanical treatments can be used to reduce the effect of PPBs by breaking the continuous network in powders as well as post-HIPped samples [54,55]. Oscillatory-pressure-assisted routes, such as hot oscillatory pressing

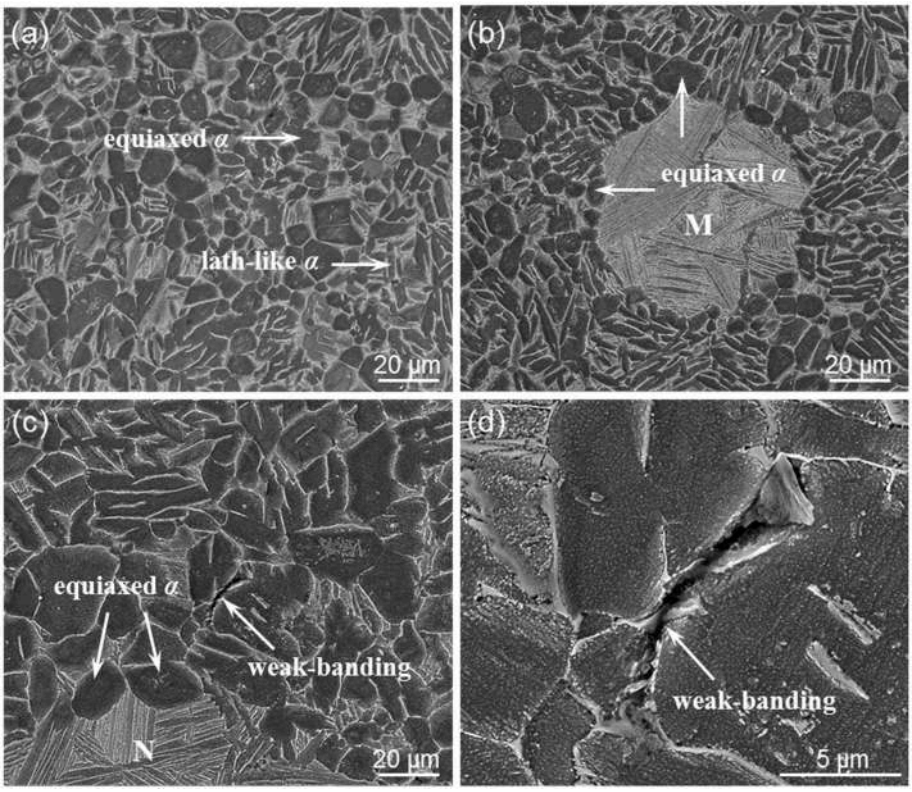


Fig. 9. Microstructure of HIPped PIII sample (a) similar microstructure as HIPped PI sample, (b) the lamellar region represented as M, (c) the lamellar region is represented by N and weak bonded area by the arrow, and (d) shows the weak bonded area at high magnification [49].

(HOP) [56] and hot oscillatory forging (HOF) [57], have been shown to effectively fragment PPB networks through enhanced localized plastic deformation and shear strain, promoting partial dissolution and redistribution of PPB precipitates and leading to a transition from inter-particle to transgranular fracture behavior, with markedly improved tensile ductility and stress-rupture life. More recently, Gaikwad et al. [58] also used powder forging as a mechanical consolidation route for PPB mitigation. The application of a triaxial stress and severe shear deformation during forging effectively fractures oxide layers and carbides decorating on particle boundaries, resulting in near-full-density components with largely eliminated PPB networks and near-isotropic mechanical properties in IN718 superalloy.

Finally, beyond purely mechanical approaches, Qin et al. [59] used an innovative pulsed electric current treatment at relatively low temperatures, i.e., 800-850 °C, on nickel-based superalloys for the dissolution of PPBs, while preserving the alloy's near-net-shape advantages and simplifying processing, as shown in Fig. 10.

In this section, different techniques for reducing PPBs have been discussed, spanning powder-surface refinement, consolidation-stage modifications, and post-processing treatments. Powder-level

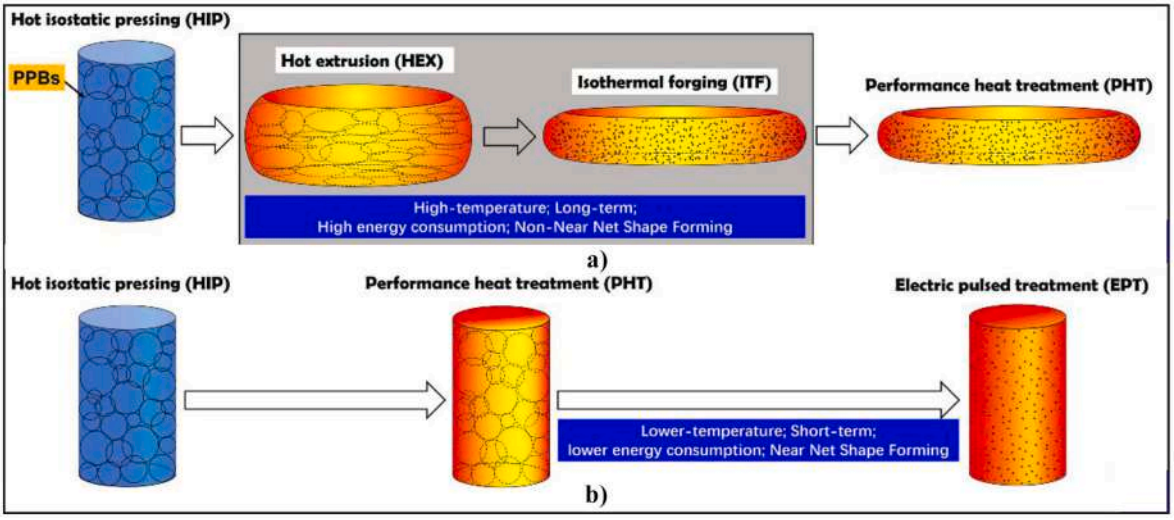


Fig. 10. Schematic diagrams of the a) traditional (hot extrusion and isothermal forging) treated and b) pulsed electric current-assisted processes for the powder superalloys [59].

approaches are effective in minimizing surface oxides before consolidation, but at the expense of complexity and cost. Mechanical and thermomechanical treatments are also highly effective in disintegrating the PPB networks; however, these approaches generally require high temperatures and additional deformation steps, due to which post-heat treatments may be required to get the desired final microstructure, which can compromise the near-net-shape and lean manufacturing advantage of HIP. In contrast, pulsed electric current treatments have recently been demonstrated to enable rapid dissolution of chain-like PPBs at relatively low temperatures through electromigration-enhanced atomic diffusion and localized high current density at PPB gaps, while largely preserving the γ' phase and grain boundary carbides. As a result, pulsed electric current processing offers a particularly attractive pathway for PPB elimination when retention of near-net-shape geometry, reduced thermal exposure, and simplified processing are required. Overall, the best PPB-mitigation strategy depends on multiple factors, i.e., alloy chemistry, component geometry, final product requirements, and cost, and may involve a combination of techniques and controls at different steps of the process.

3.2.4. Effect of the size of particles

In a study by Bassini et al. [60], the physical and chemical properties of powders and their impact on HIPping were examined, focusing on the particle size distribution (PSD) in nickel-base superalloys. It was observed that the smaller size particles, ranging from 10 to 63 μm, hinder the flowability of the batch due to high cohesion energy. Moreover, as the particle size reduces, oxygen content will increase, due to which oxides (Preferably Aluminum oxide due to the different Gibbs formation energy of the oxides) and carbides quantity on PPBs increase. However, removing these particles from the batch also affects the yield of the powder. Similarly, in the case of carbon, it was observed that the smallest and the largest exhibit higher percentages compared to the mid-range particles. However, Nitrogen and Sulphur seem unaffected by the size. Hydrogen is present only in less than 20 μm powders due to their ability to form $Ni(OH)_2$ on the surface, having high surface energy [61,62]. It was also observed that as the particle size increases, the localized hardness value also increases due to the Ti's segregation, resulting in non-uniform properties in the final HIPped part. This segregation was due to the slower cooling of larger particles as compared to the smaller ones. Therefore, choosing the particle size between 20 and 110 μm will reduce oxidation, precipitates on PPBs, and segregation of elements as observed in larger particles, overall improving the mechanical properties of HIPped parts. Similarly, the relation between the oxide layer and particle size in 316L stainless steel was also evaluated by Fleischmann, B. et al. [24]. It was observed that with the decrease in size, the oxygen content increases, and so does the oxide layer thickness. Furthermore, oxidation can also continue after the atomization process; therefore, proper storage is required to prevent further oxidation and an increase in the thickness of the oxide layer, which deteriorates the mechanical properties in post-HIPped parts. Similarly, many other researchers also observed the same results, concluding that medium-size particles ranging from 50 to 100 μm are ideal for NNS-HIPping, neither favoring the oxidation nor the segregation [63,64].

Various powder production methods offer unique benefits and challenges in terms of cost, particle size distribution, morphology, and purity. The presence of prior particle boundaries (PPBs), surface oxidation, segregation, and impurities can severely affect the mechanical properties of HIPped parts, necessitating process optimization and surface refinement techniques. Moving forward, continued research is required to improve powder yield, reduce oxide formation, and achieve optimum particle size distribution, particularly for high-performance applications in industries such as aerospace, defense, and medical implants.

4. Capsules

Capsules are the key component in the HIPping process. The success of the HIPped part relies strongly on the properties and design of capsules, which are crucial in shaping the final component while preventing contamination. Furthermore, this step can also be called the economic driver of the process [65]. Capsule manufacturing involves container sheet cutting and forming, assembling, degassing, and welding [66]. Tungsten inert gas (TIG) welding is commonly used to fabricate capsules. Still, some researchers have also discussed the advantages of laser welding, such as small spot size, low distortion, and easy accessibility to complex shapes. However, it also has some drawbacks, like trained staff, expensive equipment, etc. [67]. Varied materials and types of capsules can be used depending on multiple factors, mainly the powders enclosed and the final application. It was observed that the flat lid capsules showed 32% failure, due to which lip-shaped lids were used with a vacuum pipe to bake and vacuum the powder before sealing [18]. However, all capsules used must have the following characteristics.

- Enough strength to maintain shape and dimension during filling and degassing.
- Ductile at HIP temperature to transfer pressure on the powder to attain the desired shape.
- Compatible with the powder.
- Good weldability so that it can be completely sealed.
- Removable after HIPping.

After capsule fabrication, filling of the capsule is done, which is again a complicated process as already discussed and should be carefully optimized to achieve enough green density, minimizing the non-uniform shrinkages, and near theoretical density can be achieved after HIPping.

4.1. Materials used for capsule fabrication

The most common types of materials used for capsules are steel and glass. However, other metals like titanium, tantalum, etc., capsules are also used for the HIPping of refractory metals due to their high melting and HIPping temperatures [68,69]. Traditionally, metallic capsules with 2-3 mm thickness, made of stainless or mild steel, are used for capsules due to their cost, weldability, and mechanical properties. S. Riehm et al. [70] experimented with capsules with wall thicknesses ranging from 0.3 mm to 2 mm, and it was observed that if the wall thickness is reduced by more than 1 mm, it will be difficult to weld the capsule, resulting in defects or leakage at the joining surfaces. If the capsule is not properly closed or sealed, the argon gas will enter the capsule during the HIPping process, and it will induce gas porosity in the material. In extreme cases, the capsule can explode when the pressure is released. This happens because the pressure inside the chamber decreases more quickly than inside the capsule, and the pressure difference will result in an explosion [15]. Furthermore, the capsule's thickness should be enough to withstand pressure and temperature, especially during the initial stages of the HIPping.

As an alternative to metal capsules, glass capsules can also be used with several advantages. Some of the common benefits are easy removal, non-reactivity, high transparency, more isotropic properties, and cost-effectiveness. Borosilicate glass [28] and quartz glass [71] are commonly used as encapsulation materials due to their high thermal resistance, low reactivity, and transparency, which allows for protection against contamination. These glass capsules can be effectively used for processing metals like titanium, nickel-based superalloys, and ceramics like zirconia and silicon nitride [71,72]. Recently, Hossam Elrakayby and Kitae Kim [28] also explored the effect of borosilicate glass capsules for the HIPping of metal powders instead of conventional metal sheets. It was observed that the glass produces more isotropic shapes after

HIPping due to no stress induced by the capsule. However, when the metal capsule is used, it produces deviatoric stress due to welding at the capsule edges and the rigidity of the metal. Moreover, it was also reported that the axial densification in the metal capsules is larger as compared to the radial. However, in the case of the glass capsule, the isotropic densification was observed, and the value of k was approx. equal to 1, known as the deformation behavior [73], and can be represented as

$$K = \ln(H/H_o) / \ln(R/R_o) \quad (2)$$

Furthermore, glass capsules, along with other advantages, are easy to remove after the HIPping process is completed, as discussed in the next section. However, multiple methods are used for the removal of metallic capsules, which are time-consuming and increase the cost of the process.

4.2. Capsule removal techniques

After HIPping, capsules must be removed to reveal the encapsulated component. The removal of capsules after the HIPping is a critical step in ensuring the final product's quality. The removal process depends on the capsule material, its interaction with the encapsulated substance, and the geometric complexity of the final product. Common methods include mechanical machining [69,74], chemical etching [75], or both, which remove the capsule material selectively. Metals such as stainless steel or low-carbon steel may undergo diffusion of elements (e.g., carbon, oxygen, or nitrogen) during HIP at high temperatures to and from the HIPped part. This diffusion can alter both the material's microstructure and surface chemistry; therefore, precise removal of the surface is required to avoid contamination and alteration in the final properties of the part. However, removal of the glass container is comparatively easy and can be performed by simply breaking the glass. Bassini et al. [76] investigated this phenomenon and observed that the diffusion of carbon and other elements occurs between the capsule and the powder, resulting in a change in microstructure following degradation in the properties of the final component. The acid leaching completely removed the steel capsule and somewhat the diffusive layer of iron and carbon into the nickel layer up to 30-35 μm, confirmed by the deteriorated pictures through the microscope. In the study, it was suggested that removing the 500 μm layer can restore the material properties of the core of the sample. Furthermore, it was also observed in his study that if only a 100 μm outer layer is removed, it will restore all its mechanical properties comparable to the core, except the ductility due to the presence of PPBs and intense carbides, as summarized in Fig. 11.

It was also noted that the profile of the powder was mimicked by the surface of the sample at the initial stages of HIPping. It was because of the high hardness & strength of the powders that created the indent on the capsules and copied its profile. This indentation results in poor surface finishing after the removal of the capsule from chemical etching. However, this surface roughness can be managed by machining or other surface finishing techniques. In another study by Lebio Yang et al. [77] it was observed that the diffusion of C and Fe from the low carbon stainless steel capsule to the HIPped nickel super alloy FGH4096 M and vice versa. It was noted that the diffusion of Fe from stainless steel is greater than compared of nickel from nickel superalloy because of the higher diffusion coefficient. Furthermore, as the iron diffuses to the nickel super alloy, it changes the microstructure and so its mechanical properties. The results show that as the Fe content increases, it will diminish the gamma prime near the interface, but moving away from the interface decreases the iron content to 9.2%, resulting in the formation of fine gamma prime and then cubical gamma prime particles with further decrease. Moreover, it was also observed that the hardness varies over the distance from the interface. As distance increases, the value first decreases and then increases due to the presence of fine gamma prime particles, and as further moving away from the interface, it again decreases due to the coarser grains. It was also noted that with the distance of 400 μm, the value became constant at 425 HV, which complies with the result of Bassini et al. [76], which gave the value of 500 μm after which the mechanical properties of the surface became approximately equal to that of the core.

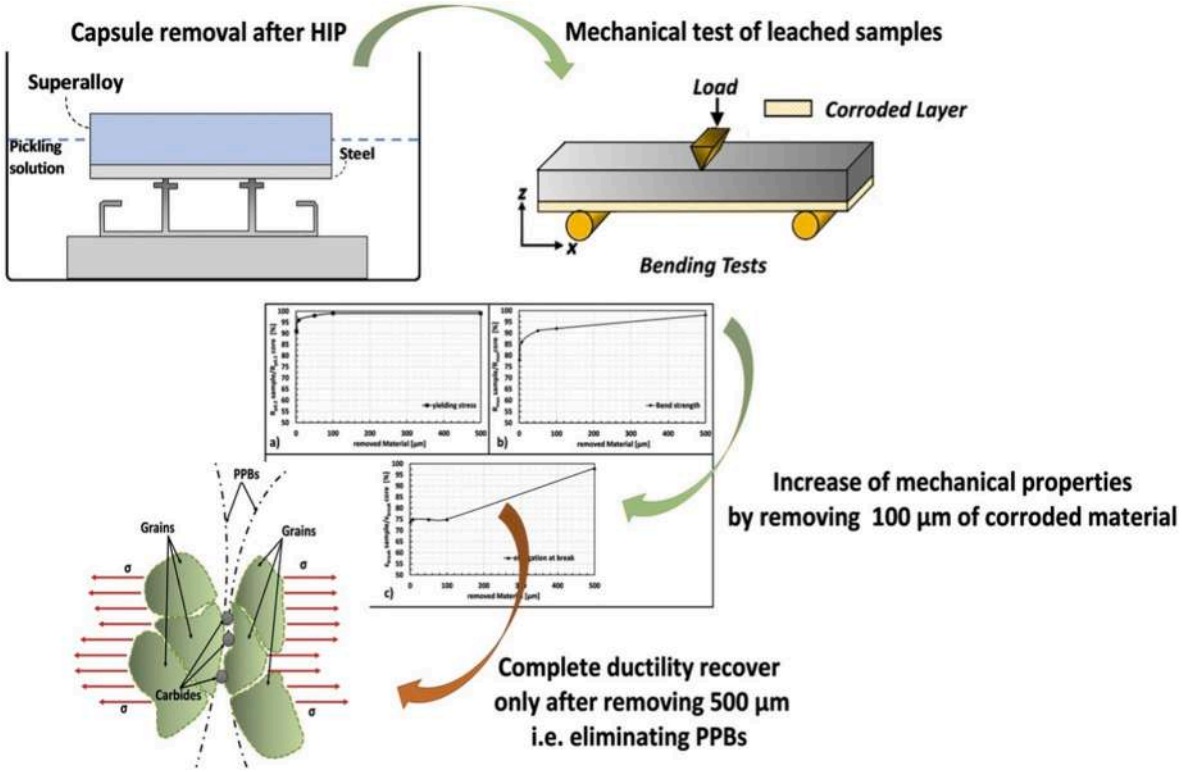


Fig. 11. Influence of chemical etching for capsule removal on mechanical properties [76].

4.3. Limitations and future perspectives

Common limitations in capsule design and the attainment of near-net shape are its non-uniform shrinkage and geometric distortions of capsules during HIPping. To mitigate these issues, one of the preventive strategies to minimize distortion is the use of computer-assisted modeling. Additionally, undue deformation in capsules resulting in shape change in the final product can be controlled by directed deformation capsules. This type of capsule can be made by increasing thickness or the addition of non-deformable elements in a specific direction, where deformation is not required, restricting deformation in specific directions [29]. Another method is to heat treat the material of capsules, which will homogenize the properties, ensuring uniformity in mechanical and thermal behavior under high-pressure and high-temperature conditions, especially for cold-formed or additively manufactured capsules resulting in anisotropic properties.

Recently, researchers have also focused on developing techniques to eliminate the need for capsules, thereby reducing costs and process complexity. For instance, research has demonstrated that employing cold pressing to the powder to achieve the required density so that the open porosity is eliminated, followed by HIPping, can achieve full densification without the need for conventional capsules known as capsule-free HIPping (CF-HIPping) [78,79]. Moreover, the innovative approach of combining AM with the NNS-HIP process is also under investigation. Because the capsules produced by manual fabrication have limitations regarding geometric complexity. By integrating different manufacturing techniques, greater flexibility can be achieved in the design and complexity of capsules. Riehm et al. [70] examined the capsules produced using the LB-PBF technique, which were filled with similar and different powders as the capsules to manufacture composite and monolithic parts, as shown in Fig. 12. This process can also be used as an alternative to cladding. However, the capsule produced by the AM technique exhibits anisotropic properties that need to be taken care of using the methods already discussed. Later, Mirz et al. [80] also used AM for the fabrication of capsules and studied the joining of evacuation tubes using TIG welding and brazing methods. With the roles of powder characteristics and capsule design established, the following section examines how these factors manifest across different metallic systems commonly processed by NNS-HIP

5. Metallic materials processed by NNS-HIP

High-end applications require materials with superior properties, but these materials are often difficult to manufacture via traditional methods. However, NNS-HIP offers solutions to longstanding challenges associated with conventional methods. Recently, high-performance metals such as stainless steel, tool steel, titanium alloys, nickel-based superalloys, and refractory metals produced via NNS-HIP have gained attention due to their exceptional properties and increasing demand in various industries, particularly in sectors including aerospace, biomedical, oil and gas, automotive, and energy.

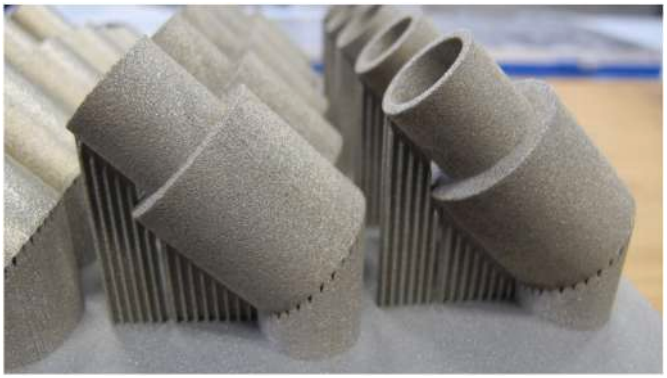


Fig. 12. 316L capsules made using L-PBF [81].

To enable a direct and consistent comparison between NNS-HIP and other manufacturing routes, i.e., casting, forging/wrought processing, and additive manufacturing, both microstructural and mechanical properties must be considered. Key microstructural parameters reported in the literature include grain size and morphology, residual porosity and pore size distribution, PPB networks and associated oxide or carbide decoration, and inclusion populations. These features govern tensile ductility, fracture toughness, fatigue resistance, and creep behavior, and therefore provide a robust basis for cross-process comparison. Compared with casting, NNS-HIP typically suppresses macro-segregation and shrinkage defects [68]; compared with wrought processing, it enables improved shape complexity and isotropy [69]; and compared with additive manufacturing routes, consolidation via NNS-HIP promotes near-full densification and closure of powder-related defects in consolidated parts [70]. However, PPBs and oxygen-derived inclusions remain process-specific limitations that can locally degrade mechanical performance if powder chemistry, storage conditions, HIP parameters, and post-HIP treatments are not adequately controlled [71].

5.1. Stainless steel

HIP has been used successfully to produce stainless steel components since 1985 in multiple applications, including turbines, boilers, centrifugal separators, etc. Almost every type of stainless-steel alloy can be produced by NNS-HIP. However, only high-grade steels (duplex or austenitic stainless steels, etc.) with good corrosion resistance and superior mechanical properties are manufactured using NNS-HIP due to the cost considerations for industrial applications. Typically, a pitting resistance equivalent (PRE) of >32 is required for offshore and other superior applications [19]. The steels, produced via HIP, demonstrate high PRE values, highlighting HIP's role in enhancing properties through refined microstructures and reduced porosity. Common grades of stainless steel with the process parameters produced by NNS-HIP are summarized in Table 1.

Due to the use of powders in NNS-HIPped parts, the role and study of oxygen have gained much importance. Initially, a study by Rao, G. A., & Kumar [89] observed that the stainless steel produced by NNS-HIP has superior mechanical properties to conventionally produced stainless steel. The exceptional properties of PM HIPped stainless steel were attributed to the low oxygen content (contrary to future studies), fine microstructure, and homogeneity. Later, Cooper et al. [91] studied the forged and HIPped austenitic stainless steel impact behavior and concluded that the toughness at below ambient temperatures in HIPped steel is much lower than its counterpart. The decrease in toughness below ambient temperature was observed in both HIPped and forged

Table 1
PM-HIP parameters in different stainless steels.

Material	HIP Temperature (°C)	HIP Pressure (MPa)	HIP Time (h)	Ref.
AISI 316L	1150	150	3	[82]
AISI 316 L	1150	105	3	[83]
AISI 316 L	950, 1000, 1050, 1120, 1160	103	4	[84]
AISI 316 L	1030	60-120	2	[85, 86]
AISI 316 L	1125	50 & 100	-	[87, 88]
AISI 316 L (CF–HIP)	920	103	2	[85, 86]
AISI 316 L (CF–HIP)	920	103	2	[87, 88]
AISI 304	1100 & 1200	100 & 120	3	[89]
Borated Stainless Steel (BSS) 304B7	1100	100-200	-	[90]

stainless steels due to the formation of stress-induced martensite near the fracture surface. However, the toughness of HIPped stainless steel at −196° was much lower than that of forged steel. As stress-induced martensite was present at the fractured surface in both types of steel, the difference was in the presence of microporosity. Therefore, it was concluded that the micro-porosity, accompanied by a larger oxygen content in the HIPped materials, depreciates the toughness of the HIPped materials at lower temperatures. However, the role of oxygen and its effect on porosity, resulting in depleting toughness, was still not clear. In this regard, a study by Cooper et al. [92] was performed, in which detailed metallographic and mechanical examinations of samples with varying oxygen contents were conducted. It was observed that the increase in oxygen content increased the porosity in the microstructure, as micro-porosity resulted from the removal of non-metallic inclusions formed by oxygen during grinding and polishing, ultimately deteriorating the material's toughness and ductility. Therefore, it was suggested that the oxygen content should be between 30 and 60 ppm to avoid the presence of a significant volume fraction of nonmetallic oxide inclusions affecting material toughness.

More recently, Cooper et al. [22] also observed that oxygen has little or no impact on yield and ultimate tensile strength, as confirmed through the comparison of experimentally and theoretically calculated values using a regression formula derived by Irvine et al. [93] for yield and UTS of stainless steel:

$$\sigma_y = 15.4\left[4.4 + 23C + 1.3Si + 0.24Cr + 0.94Mo + 1.2V + 0.29W + 2.6Nb + 1.7Ti + 0.82Al + 32N + 0.16\,(\delta - ferrite) + 0.46\,d\,e - \frac{1}{2}\right] \quad (3)$$

$$\sigma_{uts} = 15.4\left[29 + 34C + 84N + 2.7Si + 1.2Mo + 2.1Al + 3.6\,Nb + 1.9\,Ti + 0.82Al + 0.13N + 0.16\,(\delta - ferrite) + 0.9\,d\,e - \frac{1}{2}\right] \quad (4)$$

These regression equations were originally developed for austenitic stainless steels within typical compositional ranges and are applicable to room-temperature tensile loading. They are intended to estimate yield strength and ultimate tensile strength as functions of alloy chemistry and grain size, and do not account for fracture toughness, ductility, fatigue behavior, or elevated-temperature properties.

Accordingly, grain size, nitrogen, and carbon content are the dominant parameters governing yield strength and ultimate tensile strength in NNS-HIPed stainless steels. In contrast, oxide inclusions and PPB related defects exert only a limited influence on these strength properties but play a critical role in controlling fracture behavior and ductility. As also demonstrated Momeni et al. [94], the presence of inclusions and micro-porosity promotes early nucleation of voids, leading to a reduction in fracture toughness in HIPped stainless steels compared with forged stainless steels, despite similar tensile strength levels.

These findings indicate that, while yield and ultimate tensile strength of NNS-HIPed stainless steels are often comparable to those of wrought counterparts, differences in toughness and ductility exist due to the inclusion population, micro-porosity, and PPB-related defects, highlighting the importance of powder quality to achieve mechanical performance equivalence with conventionally processed stainless steels as discussed in the powder section.

5.2. Tool steel

Tool steel's high hardness, toughness, and wear resistance make it an ideal candidate for cutting applications. Among tool steels, high-speed steel (HSS) is mostly fabricated using NNS-HIP. The World's first powder atomization process was developed jointly by ASEA AB and Stora Kopparberg AB in 1969, known as the ASEA Stora Process (ASP) [95]. Later, this technology was used to produce high-speed steel called ASP tool steel [96]. The exceptionally superior high-temperature mechanical properties are attributed to the presence of a martensitic matrix with finely distributed precipitates, i.e., carbides, uniformly in the matrix [97,98]. Some of the NNS-HIPped tool steels, along with their

Table 2
PM-HIP parameters in different tool steels.

Material	HIP Temperature (°C)	HIP Pressure (MPa)	HIP Time (h)	Ref.
HSS	1200	40	0.5	[98]
HSS (PMHS 3-3-4)	1100	100	4	[103]
HSS (PM23)	1150	130	3.5	[104, 105]
HSS (M3:2)	1150	150	3	[106, 107]
Hot work steel (X40 CrMoV 51)	1150	100	3	[106, 107]
Tool steel compounds (Vanadis 10/316L & Vanax 75/316L)	1150	100	3	[105, 108]
Tool steel composite	1100	100	3	[109]
Tool steel (D7)	1000	30 & 50	4.2	[104, 108]
Tool steel (T15)	1195, 1130	104	-	[109, 110]

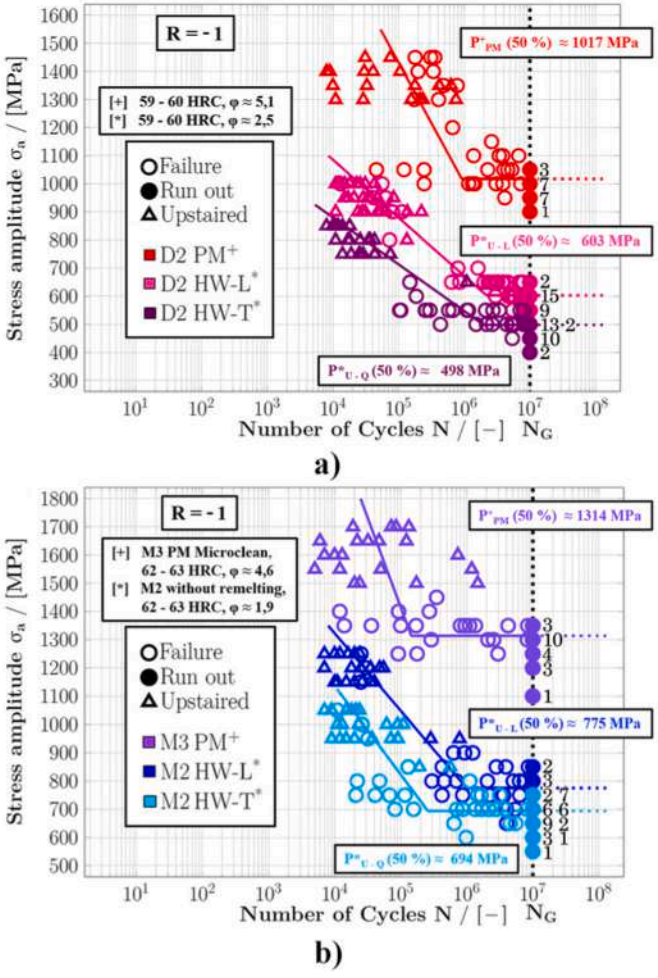


Fig. 13. Statistically evaluated S–N curves for a) Cold-Work Tool Steel (D2), b) High-Speed Steels (M2/M3) [102].

parameters, are presented in Table 2. Furthermore, it was observed that the HIPping produces a finer and more uniform distribution of carbides in HIPped tool steel as compared to the conventional methods, giving it superior properties. Recently, Furuya et al. [99] demonstrated that the HIPped Cr–Mo–W–V–Co High-Speed Steel showed 44% and 58% increases in strength and impact values, respectively, as compared to conventional techniques. Suggests the NNS-HIP process as an ideal candidate for HSS in compliance with the previous results [100,101]. More recently, Scholl et al. [102] also compared the high-cycle fatigue (HCF) of tool steels produced by NNS-HIP and hot-working. Fig. 13 compares the HCF behavior of NNS-HIP and hot-worked tool steels under fully reversed loading conditions (R = −1) presented as S–N curves. In both cases, NNS-HIP steels (D2 PM and M3 PM) exhibit higher fatigue endurance limits and reduced scatter compared with their hot-worked counterparts (D2 HW and M2 HW), as indicated by the higher 50% survival probabilities (P*). The observed scatter in fatigue life is mainly due to the defect populations rather than intrinsic microstructural parameters. NNS-HIPped steels show delayed fatigue crack initiation due to the smaller number of critical defects. In contrast, hot-worked steels exhibit earlier crack initiation at lower stress amplitudes, associated with larger and more heterogeneous defect populations. Overall, these results confirm that the HCF performance of tool steels is predominantly defect-controlled, in agreement with defect-sensitive fatigue models for powder-metallurgy and NNS-HIP-consolidated steels, where the endurance limit is governed by extreme-value statistics of the largest defect present.

5.3. Titanium alloys

Titanium alloys are generally used in oil and gas exploration, power generation, and aerospace applications where the temperature is between 400 and 600 °C, providing excellent mechanical and corrosion-resistant properties. Titanium using HIP technology was first developed in the 1970s and adopted by multiple companies like Crucible Research (USA) and Tecphy (France), and they use these parts in various applications, including jet and rocket engines, as also shown in Fig. 14 [14].

The HIPping temperature for titanium alloys mainly depends on the beta transus temperature. Mostly Ti alloys are HIPped between 900 and 930 °C with a pressure commonly of 120 MPa. This temperature range promotes the formation of fine-grained α + β microstructures, which are known for their superior mechanical properties, including strength and fatigue resistance. While some alloys, such as Ti–5Al–5V–5Mo–3Cr near beta alloys, are HIPped at lower temperatures at approx. 800 °C. A few common alloys of titanium, along with their process parameters, are tabulated in Table 3. HIPping temperature is important as it determines the microstructure, resulting in the final properties of the alloy [111]. Furthermore, the use of HIP technology for titanium alloys reduces the dwell fatigue effect that occurs under cyclic loading with elongated peak stress time periods. This phenomenon is mainly due to microstructural anisotropy, where soft alpha-phase grains deform more than hard grains, resulting in stress concentrations and promoting crack initiation. This type of fatigue is common in high-strength grades like Ti–6Al–4V of titanium alloys when used in aerospace applications at high temperatures [49].

Overall, when compared with wrought titanium alloys, NNS-HIPed titanium components exhibit improved microstructural isotropy and significantly reduced internal porosity, features that are particularly beneficial for fatigue-critical aerospace applications. Nevertheless, fatigue performance remains strongly governed by the size and distribution of residual defects rather than by average porosity alone. Therefore, NNS-HIP significantly narrows the performance gap with wrought titanium alloys, achieving fatigue resistance comparable to or potentially exceeding that of conventionally processed materials, bound to the control of powder quality, defect population, and the application of optimized post-HIP heat treatments.

Table 3
PM-HIP parameters in different titanium alloys.

Material	HIP Temperature (°C)	HIP Pressure (MPa)	HIP Time (h)	Ref.
Ti6Al4V	930	120	3	[112]
TA15 Alloy	910-970	120	3	[113]
Ti–6Al-4VELI	940	120	3	[114]
Ti–47Al–2Cr–2Nb	1020,1050,1100,1150	120	3	[115]
Ti-43.5Al-6.5Nb-1.5Cr-0.5C	1150	120	3	[116]
Ti6Al4V	930	120	3	[75]
Near α-Ti Alloy	900,950,1000	120	3	[117]
Ti6Al4V Alloy	930	100	3	[118]
Ti–6Al–4V	880, 930, 980	100	4	[119]
Ti–6Al–4V	930	100	4	[120]
Ti–6Al–4V	950,1000,1050	120	3	[121]



Fig. 14. Titanium engine housing fabricated via NNS-HIP [14].

Table 4
PM-HIP parameters in different nickel alloys [7].

Material	HIP Temperature (°C)	HIP Pressure (MPa)	HIP Time (h)	Ref.
Inconel 718	1200	120	3	[60, 123]
Inconel 718	3 steps: (1) 1100–1200 (2) 1220–1260 (3) 1090–1130	>120	3 steps: (1) 1–2 (2) 0.2–2 (3) 2–6	[124]
Inconel 625	1160	120	4	[125]
Inconel 625	1100	110	3	[126]
Inconel 625	1150	100	3	[127]
Inconel 625	1160	120	4	[128]
Inconel 600	1200	140	3	[129]
Inconel 718	1180	170	3	[130, 131]
Ni-based superalloy	1190	120	3	[132]
FGH97	1200	150	3	[63]
FGH96	1120	120	4	[133]
FGH4096	1160	150	4	[134]
RR1000	1180	100	4	[135]
CM247LC	1260	150	2	[64]

5.4. Nickel-based superalloys

Nickel-based superalloys are widely used in aerospace and power-generation applications operating above 800 °C, where high strength, creep resistance, and oxidation/corrosion resistance are required. Their exceptional performance are due to the complex and multiple alloying elements, including solid-solution strengthening by Mo, Cr, Co, and W, precipitation strengthening by Al and Ni resulting in the formation of γ' (Ni_3(Al, Ti)) and γ'' (Ni_3Nb), and the presence of MC-type carbides and stable oxides due to the C, Cr and Mo, which together enhance the creep resistance up to ~70% of the melting temperature, compared with ~30–40% for conventional structural alloys [122]. Due to the exceptionally high strength and superior properties, the fabricability becomes an issue for these alloys, due to which they are typically fabricated via NNS-HIP at 1100–1260 °C under pressures of 100–170 MPa, followed by solutionizing and aging heat treatments depending on the final application. Solution treatment may be conducted below the γ'/γ'' solvus (sub-solvus) to retain a fine-grained microstructure with improved tensile strength and fatigue resistance, or above the solvus (super--solvus) to dissolve strengthening precipitates and promote grain growth, which will enhance creep resistance but reduce yield strength and ductility. Also, Super-solvus solutionizing can partially disrupt and redistribute PPB-related precipitates through enhanced diffusion, as the grains grow beyond the PPBs, although it is generally insufficient to fully eliminate PPB networks without additional mechanical or thermo-mechanical processing, as discussed. The time, temperature, and pressure conditions employed for various nickel-based superalloys processed by NNS-HIP are summarized in Table 4.

Recently, nickel-base metal matrix composites (Ni-MMCs) have also been developed to improve the mechanical properties of turbo pump mechanical seals for aerospace applications using NNS-HIP, in which IN625 alloy was reinforced with varying volume fractions (5%, 10%, 25%) of SiC and TiB_2, as shown in Figs. 15 and 16 [128].

Similarly, Ni-rich 60NiTi shape memory alloys were also successfully produced using NNS-HIP, and the effect of mechanical alloying to achieve a homogeneous microstructure was also studied [136]. Despite the excellent mechanical properties of nickel super alloys, oxygen content resulting in the formation of PPBs is an issue for the nickel super alloys, as documented by multiple studies discussed in the powder section in more detail.

5.5. Refractory metals

Refractory metals, such as niobium, tantalum, tungsten, etc., have high melting points (above 2000 °C) with excellent mechanical properties, making them ideal for many high-temperature industrial applications, i.e., aerospace, nuclear, and chemical applications. Mostly refractory metal parts are produced using PM techniques owing to their cost, poor machinability, and high-temperature molding. The pressure during HIPping of these metals typically ranges from 100 to 200 MPa, while the temperature varies based on the processed material properties. For tungsten-based alloys, temperatures range between 1000 and 1500 °C, while tantalum and its carbides require 1000 to 1200 °C. Niobium alloys are processed around 1100 °C, and molybdenum-based composites operate from 1200 to 1500 °C, as tabulated in Table 5.

In past years, refractory metal powders were consolidated into a final shape via conventional PM methods and sintered, and further density was increased via mechanical working. However, now using HIP, near theoretical density can be achieved by applying temperature and pressure simultaneously. In addition, NNS-HIP also prevents the powder from encountering the environment at elevated temperatures by using sealed capsules. Furthermore, as indicated in Table 5, metals and their composites can be HIPped without using a can in an inert atmosphere by prior uniaxially or cold isostatically pressing the powder, making the process more economical. Mostly cold isostatic pressing (CIP) or sintering is done before final HIPping for the refractory metals for better consolidation. Comparative studies demonstrate that these pre-consolidation routes (CIP–HIP, sinter–HIP, and direct HIP) significantly influence the final grain size and residual porosity of refractory metals. Larger grains are typically observed in sintered compacts compared to CIPed powders prior to HIPping; nevertheless, theoretical densities exceeding 99 % can be achieved using both approaches [69, 150]. Moreover, previously, tantalum was also HIPped directly from the powder, but the grain size was greater than pre-processed powders, i.e., approx. 60 μm [151]. This observation further confirms that introducing CIP or sintering prior to HIPping effectively suppresses grain coarsening and improves the resulting microstructural uniformity and properties. Likewise, CIP followed by HIP is also used to consolidate the rhenium powder for the production of a combustion chamber for aerospace applications. In the study by Leonhardt et al. [152] the density of 95-98 % was achieved after CIP, followed by sintering, and then HIPping was used to achieve 99.9 % density. Using CIP + HIP has reduced the manufacturing cost of such chambers by 35 %, time by 30 - 40 %, buy-to-fly ratio to 70 %, and machining costs to nearly 50 %, highlighting the industrial advantages of combining pre-HIP consolidation with near-net-shape HIP for refractory metal components.

Overall, while near-net-shape HIP enables near-theoretical density and the fabrication of complex geometries that are difficult to achieve via conventional sintering or forging, its full benefits in refractory metal systems are maximized when combined with optimized powder conditioning and appropriate pre-HIP consolidation strategies to control grain growth and eliminate residual or surface-connected porosity.

This trend is clearly reflected in the HIP processing windows reported across different metallic systems, as summarized in Fig. 17, where refractory metals occupy the highest temperature and pressure regimes compared with steels, titanium alloys, and nickel-based superalloys. Importantly, the inclusion of pre-consolidation steps before HIPping shifts these processing windows toward lower HIP temperatures, pressures, and dwell times by reducing initial porosity and enhancing powder–particle contact, thereby improving densification efficiency.

6. Modeling of HIPping

In ideal conditions, the change in shape during NNS-HIPping should

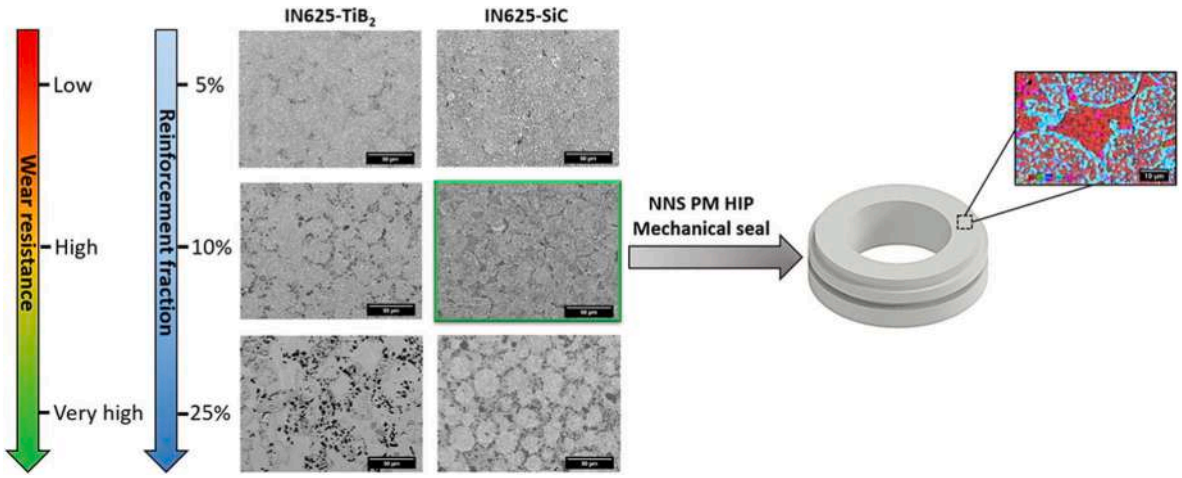


Fig. 15. Development of Ni-base metal matrix composites by NNS-HIP [128].



Fig. 16. Ni-MMCs mechanical seals after machining produced by NNS-HIPping [128].

Table 5
PM-HIP parameters for refractory metals and their composites.

Material	HIP Temperature (°C)	HIP Pressure (MPa)	HIP Time (h)	Ref.
Niobium C103 Alloy	2 steps: (1) 1260 (2) 1593	103.4	2 steps: (1) 3 (2) 3	[137]
Tantalum carbide (TaC) & Tantalum hemicarbide (Ta_2C)	1630	195	2	[138]
TaC	1600	200	1.67	[139,140]
Tantalum powder (CIP + HIP)	1500	100	2	[69,141]
W–Cu Powder	950	110	2	[139,142]
Tungsten (CIP + HIP)	1759-1900	200	3.12	[68,69]
Tungsten heavy alloy (THA) (CIP + HIP)	1450	30-45	1.5	[143–145]
W–5Cr-0.5Y (CIP + HIP)	1150-1250	170	2	[142,146]
THA (93%W-4.9%Ni-2.1%Fe) (CIP + HIP)	1300	100-150	1	[68,147]
93 W–Ni–Fe Tungsten Alloy	1400	140	2.5	[141,143,148]
WC-Co (CIP + HIP)	900-1200	150	1	[146,149]
WB4–B & WB4–B–Ta (CIP + HIP)	1350	150	1	[140,147]
W–Ta composite	1255	200	2	[141,148]
$MoSi_2$	1200-1400	207	1 & 4	[144,145,149]

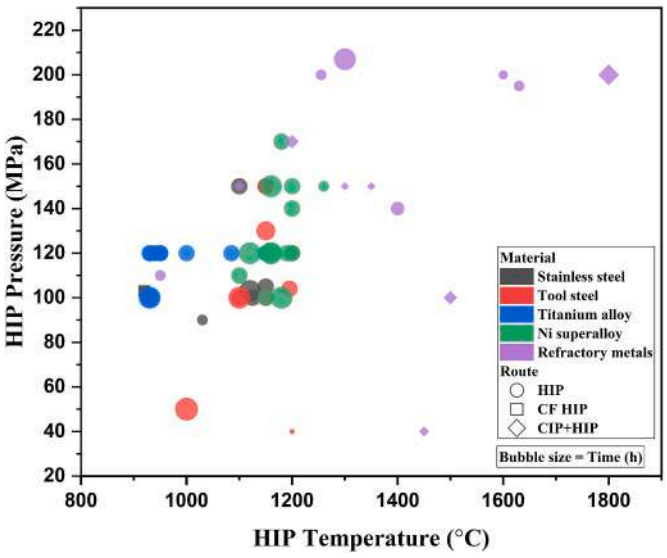


Fig. 17. Compilation of HIP processing windows reported in the literature for metallic materials processed via NNS-HIP.

be isotropic, but practically, an anisotropic change in shape and size is observed. As HIPping is a costly and complex process, the hit-and-trial method for observing the final shape can be expensive, as many factors are involved in determining the shrinkage. For example, time, temperature, pressure, and other material properties like size, creep, plastic deformation, etc. Therefore, modeling the shrinkage behavior and pore closure mechanisms under the combined influence of these parameters can save time and money and achieve predictable results for industrial use. The choice of models and their techniques depends on multiple factors, i.e., type of material, accuracy, time, and complexity. For example, elastic-plastic models are chosen to obtain faster results. In contrast, visco-plastic models require high computational efficiency because time and temperature-dependent creep behavior, i.e., creep and diffusion, increases the complexity. Porous material models are used for the accurate prediction of pore closure and densification mechanisms, while phenomenological models are employed for rapid analysis based on empirical data.

Based on the characteristic length scale at which the material behavior is represented and the dominant physical mechanisms considered during densification, HIP modeling approaches are commonly divided into microscopic, mesoscopic, and macroscopic models. This classification provides a logical framework for selecting appropriate modeling strategies depending on the objectives of the simulation, required accuracy, and computational efficiency.

These models are typically implemented using analytical formulations and numerical methods, most commonly FEM based simulations, employing commercial software such as ABAQUS, ANSYS, or COMSOL Multiphysics, as well as user-defined constitutive subroutines to describe material-specific densification behavior.

Each modeling approach addresses a distinct aspect of the HIP process: microscopic models focus on particle-scale densification mechanisms, macroscopic models predict global shape change, stress evolution, and tooling–capsule interaction, while mesoscopic models bridge these scales by capturing collective particle behavior with reduced computational cost.

There are three types of modeling approaches.

1 Microscopic: Focus on the individual particles and their environment. Microscopic modeling techniques are based on physical mechanisms regarding which Arzt and Ashby [153] developed the foundational equation.
2 Macroscopic: Based on continuum mechanics and FEM is used for its analysis. The most important factor relating to the reproducibility of this technique is the similar powder and filling method [16].
3 Mesoscopic: This type of modeling technique serves as an intermediate approach between the microscopic and macroscopic techniques by representing clusters of particles. The computational efficiency of mesoscopic models lies in their ability to provide a balance between detail and scalability, making them suitable for many practical applications without the need for excessive computational resources.

6.1. Microscopic modeling

In terms of microscopic modeling, many researchers have developed equations for predicting the final shape based on the densification mechanisms with respect to individual particles. Initially, these equations are mostly based on ideal assumptions. However, particles are not spherical, temperatures and pressures are not steady, defects like porosity can be present in the powders, etc. Therefore, to deal with these deviations, researchers have also incorporated these deviatoric factors into the equations to predict more accurate shape changes, discussed in detail by Atkinson et al. in their review article [4]. The equation proposed by Artz et al. was modified by R.D. Kissinger et al. [154] to include deviatoric stress arising from smaller particle sizes with temperature and

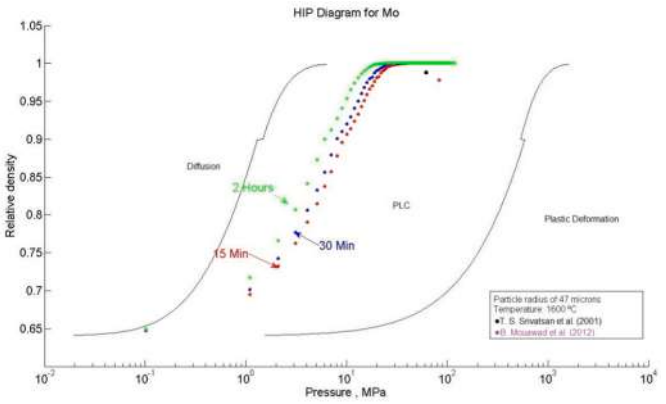


Fig. 18. Diagram for Mo with particle radius of 47 μm and temperature of 1600 °C [158].

pressure. The microscopic approach is used to contour HIP maps to predict density as a function of temperature, pressure, and time. Redouani et al. [155] also investigated the HIP process using a microscopic approach. Using random dense packing (RDP) principles with an initial relative density of 0.64 for identical spherical particles, densification maps were plotted for different metal powders, i.e., copper, nickel, and tungsten powders. The simulation results closely matched experimental data for copper, nickel, and tungsten powders, as well as for tin and lead, validating the model's accuracy. Later, Redouani et al. [156,157] also simulated the densification of other metallic powders in multiple studies and found the results coherent with the experimental data. Recently, Diego Gomez and Rodrigo Palma [158] also investigated the densification behavior of Mo using microscopic modeling techniques and used the equation developed by Arzt et al. [153], focusing on plastic densification, power-law creep (PLC), and diffusion mechanisms. The results indicate that at temperatures and pressures greater than 0.5 T_m and 15 MPa, relative densities above 0.95 are achieved, with power-law creep being the dominant mechanism and vice versa. The HIP diagrams were also made that can be used for the optimization of the HIP process for Mo and validated against other powder methods such as Spark Plasma Sintering (SPS) and Plasma Pressure Compaction (PPC), as shown in Fig. 18.

6.2. Macroscopic modeling

In the macroscopic approach, Shima and Oyane [159] in 1976 presented the plasticity theory of porous metals, which is the basis of most models. Later, Abouaf et al. [160] developed the equation for plasticity, elasticity, and thermal properties to model the mechanical deformation in the powders. After this, many models were developed for the densification and shape calculation, but most of them take too much time to calculate, making it not feasible for industrial applications. Recently, Yuan et al. [26] employed the FEM based on only plasticity theory for the determination of the final shape after HIPping using Ti–6Al–4V powder, as 90% of densification and deformation is based on instantaneous plastic deformation. The main advantage of this theory is that it involves fewer parameters, therefore, the results can be obtained quickly and show 98% coherence with experimental results, particularly for the cylindrical body. However, this method also has limitations regarding the tooling design, which cannot be achieved by a single iteration. Chung et al. [29] examined the effect of powder preparation, temperature gradient, and capsule design on the final shape using the visco-plastic model suggested by Abouaf. This method was chosen for its simplicity and efficiency in predicting shape changes for complex geometrical components with fewer parameters compared to other microscopic or mesoscopic approaches. The study concludes that the initial relative density distribution significantly affects the final shape,

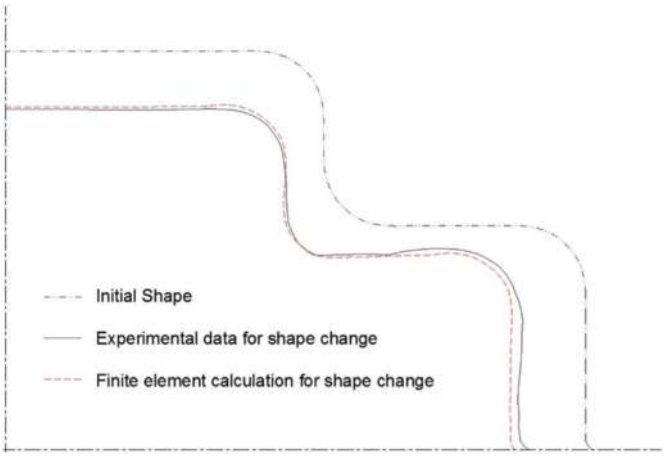


Fig. 19. Comparison between experimental data and finite element calculations for the deformed shape of nickel-chromium–cobalt alloy [161].

with thinner capsules deforming more, enabling directed deformation of capsules. Elrakayby et al. [161] also used the Abouaf et al. model for the FEM of HIPping of Nickel superalloy powder in the stainless-steel capsule. The c and f values (rheological functions) are used from the work of Abondance et al. [162] and are represented as:

$$f(D) = 0.274\ \{(1-D)/\ (D-D_o)\}\mathrm{e}\ 0.846\ \mathrm{s} \quad [5]$$

$$c(D) = 1 + 0.6\ \{(1-D)/\ (D-D_o)\}\mathrm{e}\ 0.87 \quad [6]$$

These parameters are crucial in describing the relationship between the stress state and the densification mechanisms of the powder compact. However, in this case, they were calculated for the titanium alloy but found in good agreement when used in nickel superalloy analysis due to approximately similar properties at higher temperatures. It was observed that the simulation done using ABAQUS© was in coherence with the experimental results, with a maximum error of about 3%. Therefore, this model with c and f values can be successfully used for predicting the after-HIPped shape of the nickel superalloy powder as depicted in Fig. 19.

In another study by Essa et al. [25], Gurson's pure plastic theory [163] of porous metal was used to model the densification of IN718 superalloy using FEM in ABAQUS. The results show that the thermal gradient exists between the internal and external surfaces due to the lower thermal conductivity of loose powder as compared to the consolidated. As time passes the gradient decreases due to the consolidation of powder at the core area. Similarly, the pressure is also not hydrostatic due to the tooling misses stresses, as well as the stresses developed due to the thermal gradient and expansion. Despite these factors, the model achieves a high accuracy of more than 1%, highlighting plastic deformation as the dominant densification mechanism for nickel-based alloys.

6.3. Mesoscopic modeling

This type of modeling approach lies between microscopic and macroscopic scales by focusing on the collective behavior of materials or systems at an intermediate scale, i.e., clusters. For example, during HIPping, mesoscopic parameters such as relative density functions or stacking fault energy (SFE) can be simulated by FEM, predicting the densification and deformation of metal powders. The main advantage of this modeling approach is the balance between complexity and time. Elrakayby and Kim [164] developed their model, known as the Elrakayby and Kim model, for the analysis of the densification of the nickel-based powder using a mesoscopic approach. This model is based on stacking fault energy and claims that it gives much better results as compared to the Abouaf et al. model. The c and f values were calculated using creep and compression strength tests at elevated temperatures. It was concluded that this model could predict near-net shapes for HIPping. The numerical simulations show excellent agreement with the experimental results, with an error of 1-3% based on particle size and initial relative density. Similarly, in another study, the same Elrakayby and Kim model was used with glass capsules, enclosing stainless steel and nickel powder. It was observed that the experimental data and the FEA are in good agreement except at the neck area due to the shape of the capsule. It was also concluded from the results that glass containers can produce more isostatic near-net shape parts cost-effectively [28].

Furthermore, recently researchers tried to combine the different approaches to develop multiscale frameworks, enhancing the accuracy of predictions for distortions and densification in Near-Net Shape HIP processes [165]. Recently, Elguezabal et al. [32] used a multiscale framework integrating mesoscopic FEM with a macroscopic visco-plastic model for astroloy in Abaqus. Experimental validation depicted high accuracy with errors of less than 0.2%, i.e., a deviation range of ±2 mm for a 1500 mm component. This multiscale model demonstrated superior capabilities for NNS-HIP process simulations.

The modeling of the NNS-HIP process has advanced from empirical models to sophisticated multiscale approaches with improved accuracy. However, the choice depends on the level of detail, computational efficiency, and the specific characteristics of the material required. Adequate HIP models allow the optimization of the HIP process for complex geometries. It also allows designers to get as close as possible to the finished shape, thereby eliminating expensive machining operations or avoiding any risk of undersized parts. In addition to the models for the HIP process, the database regarding the properties of powders, capsules, and inserts is needed to use the models for accurately predicting the shape of the final part and designing the capsules.

7. Recent developments

HIP technology has witnessed significant advancements over the past years, due to its growing applications and demand in various industries. These developments include the optimization of process parameters, cost reduction, new materials, integration with other technologies, advanced software tools, and enhanced equipment capabilities. Moreover, these advancements have enhanced process efficiency, predictability, and acceptance, enabling this technology to produce defect-free, high-performance, and novel parts.

7.1. Cost optimization of HIP

Almost every type of metal can be fabricated using HIP, but the process is mostly used for expensive metals, otherwise, economics will not favor the process [30]. The main utility of HIP is for high-end applications like oil and gas, aerospace, and energy, which has also increased over the years after receiving recognition from international standards like ASME, API, and NACE [66]. Moreover, in the HIPping process, two main steps are considered the most contributing factors to the overall cost, as shown in Fig. 20.

1 Consolidation
2 Encapsulation

To decrease the cost-effect ratio of consolidation, larger HIP equipment has been designed and more are in process, i.e., Giga HIP at MTC Japan [31]. Larger HIP equipment can process more parts in a single cycle and handle greater volumes, reducing the cost per unit volume. As summarized in Table 6, increasing the HIP vessel size results in a threefold reduction in processing cost per kilogram, due to higher material processed per cycle and improved equipment utilization, clearly demonstrating the strong economy-of-scale effect inherent to industrial HIPping operations. Moreover, integrating fast cooling and quenching technologies in HIP equipment has significantly reduced variable

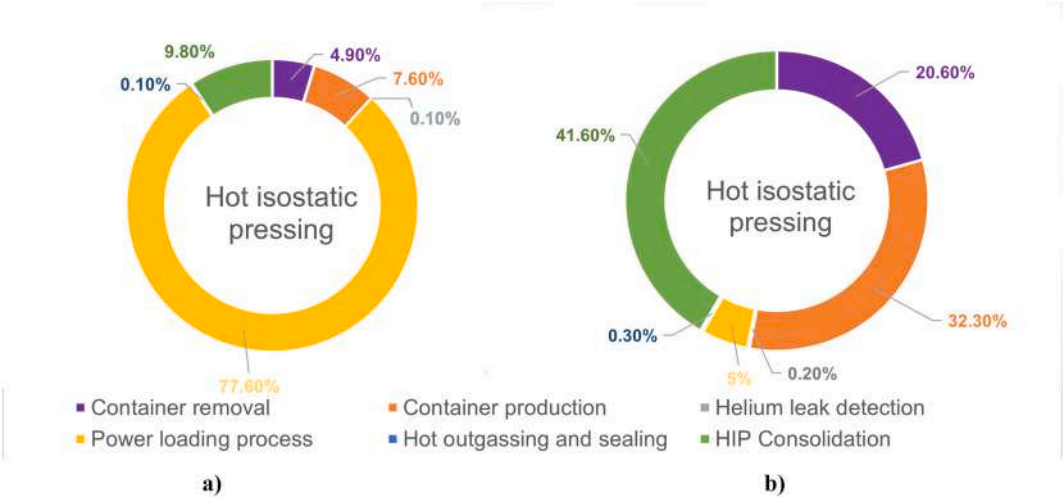


Fig. 20. Cost breakdowns for the NNS-HIPping process: a) with powder, b) without powder [65].

Table 6
Examples of HIP cost reduction using large HIP systems [166].

Parameter	Large HIP	Small HIP
HIP vessel size	Ø 1.8 m × 3.3 m	Ø 0.8 m × 2.5 m
Total cycle time	14 h	8 h
Hold time	4 h	4 h
Production per cycle	20 tons/cycle	2 tons/cycle
Annual capacity	10,000 tons/year	1800 tons/year
Processing cost	0.3 EUR/kg	0.9 EUR/kg

expenses. Additionally, the gas used in the HIPping process can be reused by storing it in a tank rather than dumping it, further improving the cost efficiency of the HIP system.

Furthermore, many researchers are trying to exclude the expensive canning step from the HIPping process to reduce encapsulation costs, making HIP more economical. It has been reported that encapsulation and its removal contribute more than 50% of the total process cost, excluding powder cost [65]. Flodin et al. [167] also examined the practical implications of canning in HIPping technology. As per the author, HIPping is not being widely used due to its expensive canning process for near-net shape. Eliminating the canning process by achieving a pre-pressed part with a density sufficient to eliminate interconnected porosity enables the remaining densification to be completed through HIPping. This approach enhances cost-effectiveness and increases the process's industrial applicability. Therefore, HIPping can be performed without the canning process, but at the expense of complexity. The experiments show that the pre-sintered and double-pressed powder exhibits the highest density as compared to single-pressed parts. However, after HIPping of the double-pressed parts, the properties were not equivalent to the forged parts. The reason was that the surface porosity was still present, which cannot be removed by HIPping. Therefore, after post-processing treatments like shot peening or machining, the fatigue strength of the components can be significantly improved, comparable to wrought alloys. Capsule-free HIPping has also been demonstrated for near-net-shape titanium components when interconnected porosity is eliminated before HIP. A comprehensive U.S. Department of Energy program report showed that press-and-sintered titanium powders with closed porosity could be fully consolidated by HIP without canning, achieving near-theoretical density and competitive mechanical properties [168].

7.2. HIP coupled with AM

Recently, many researchers have used different techniques collectively with HIP to achieve synergistic properties. Additive manufacturing with NNS-HIPping covers the shortcomings of each process by simultaneously achieving the complexity of design from AM and superior isotropic properties from the HIP. Additionally, different metallic powders and capsules have also recently been HIPped to form composites and achieve integrative properties. Horton & Sheppard [169] explored the benefits of combining NNS-HIP with AM by fabricating capsules using AM and filling them with the same powder, i.e., Haynes 282 (A-282). The results demonstrated that the produced parts had superior properties compared to traditional methods. The components also showed superior strength, hardness, and ductility as compared to parts produced from castings. Additionally, a raw material cost reduction of 40% was also observed. More recently, Riehm et al. [81] also investigated the integration of AM and HIP to produce composites from different capsule and powder materials. Furthermore, a thin-walled capsule was also optimized, produced using AM, with a wall thickness as low as 0.6 mm, to reduce the cost compared to traditional welding methods. Another approach to combining these two technologies involves printing a dense outer shell with loose powder using AM, reducing printing time and cost. Lerda et al. [170] used this approach to print Inconel 718 (IN718) using Laser Powder Bed Fusion (L-PBF), and the results were promising. It was observed that this reduced printing time by 45-60 % and porosity to 0.04%.

Moreover, the development of advanced HIP equipment, incorporating techniques such as oxygen-getter cassettes, automated bakeout functions, and clean processing atmospheres, has opened new possibilities for HIP technology by reducing oxidation and discoloration during processing. These innovations ensure better material properties and reduce the need for costly post-processing steps [171]. With more control over the HIP parameters, better properties and heat treatment processes can be achieved, making the HIP equipment a more integrated unit.

8. Conclusion

The HIPping process has proven to be a versatile and effective method for achieving near-full densification in various materials with multiple advantages, making it crucial for industrial applications.

To summarize the key findings, the following points can be highlighted.

- HIPping can achieve the complexity of casting with properties equal to or greater than the wrought alloys due to less scatter.
- Statistics and data have proven that industries have adopted HIP technology due to its economic viability, especially for complex and low-volume parts.

- Rapid cooling and quenching, safety checks, reuse of gas, better data, modeling, in situ heat treatment, improved control, clean atmosphere, larger sizes, and automation are a few updates in the HIP equipment that have made it more industrially acceptable. However, researchers are still working to improve the process further.
- Other than the equipment, improving the yield and quality of powders as the foundational building block is also equally important.
- Currently, AM and other techniques have been co-used with HIP to further enhance the properties of the final parts in terms of complexity and cost-effectiveness.

HIPping technology is evolving through research and development in every step of the HIPping cycle starting from powders to the inspection involving; the quality of powders, yield of powders, handling of powders, canning, controlling parameters, better mathematical models, efficient HIP equipment, more systematic data, reliable finishing techniques, inspection and testing, and reproducible material properties. By employing improvements in every field, HIP technology will be more market-friendly, accessible, and comparable to conventional technologies. These advancements will reduce barriers to adoption and further increase the widespread implementation in the market. Significant advancements have been made; however, areas including the development of databases and multiscale modeling techniques specific to HIP still require further progress. Improved data availability can aid in the design of processes and parameters to achieve better properties and control over microstructure during HIPping. Moreover, such data can be used in artificial intelligence frameworks to predict new outcomes, opening new avenues for exploration within this field and paving the way for innovative materials with improved properties [172].

Funding

This work was funded by the European Union – Next Generation EU, Mission 4 Component 2 - ECS00000036 - CUP [E13B22000020001]

Declaration of competing interest

The authors declare that they have no known competing financial interests or personal relationships that could have appeared to influence the work reported in this paper.

References

[1] Chu R, et al. Cracking and segregation in high-alloy steel 0.4 C1. 5Mn2Cr0. 35Mo1. 5Ni produced by thick continuous casting. Heliyon 2019;5(3):e01329. https://doi.org/10.1016/j.heliyon.2019.e01329.
[2] Wei X, et al. Influence of Process Parameters on Grain Size and Texture Evolution of Fe-3.2 wt.-% Si Non-Oriented Electrical Steels. Materials 2021;14(22):6822. https://doi.org/10.3390/ma14226822.
[3] (EPMA), E.P.M.A. Hot isostatic pressing (HIP). Available from: https://www.epma.com/what-is-pm/powder-metallurgy-process/hot-isostatic-pressing-hip/.
[4] Atkinson H, Davies S. Fundamental aspects of hot isostatic pressing: an overview. Metall Mater Trans 2000;31:2981–3000. https://doi.org/10.1007/s11661-000-0078-2.
[5] Loh N, Sia K. An overview of hot isostatic pressing. J Mater Process Technol 1992;30(1):45–65. https://doi.org/10.1016/0924-0136(92)90038-T.
[6] Bocanegra-Bernal M. Hot isostatic pressing (HIP) technology and its applications to metals and ceramics. J Mater Sci 2004;39(21):6399–420. https://doi.org/10.1023/B:JMSC.0000044878.11441.90.
[7] Javadzadeh Kalahroudi F, et al. Microstructure and fatigue behavior of PM-HIPed Ni-Based superalloys and martensitic tool steels: a review. Metals 2024;14(10):1159. https://doi.org/10.3390/met14101159.
[8] Cui J, Lv X, Fu H. Numerical simulation and hot isostatic pressing technology of powder titanium alloys: a review. Metals 2025;15(5):542. https://doi.org/10.3390/met15050542.
[9] Johannisson T, Zander K. Wire wound high pressure vessels for industrial applications. In: High-pressure science and technology: volume 1: physical properties and material synthesis/volume 2: applications and mechanical properties. Springer; 1979. p. 1633–8. https://doi.org/10.1007/978-1-4684-7470-1_201.
[10] Martelli P, Bassini E, Ugues D. The effect of hot isostatic pressing pressure level and solution annealing cooling rate on CM247 LC nickel-based superalloy processed by laser-based powder bed fusion. Progr Addit Manuf 2024:1–14. https://doi.org/10.1007/s40964-024-00645-6.
[11] Zhou Y, et al. Effects of HIP temperature on the microstructural evolution and property restoration of a Ni-Based superalloy. J Mater Eng Perform 2012;22(1):215–22. https://doi.org/10.1007/s11665-012-0246-8.
[12] Xiao Y, et al. Diffusion bonding of copper alloy and nickel-based superalloy via hot isostatic pressing. J Mater Res Technol 2022;19:1789–97. https://doi.org/10.1016/j.jmrt.2022.05.152.
[13] Ruys A, et al. Powder processing of bulk components in manufacturing. In: Handbook of manufacturing engineering and technology; 2015. p. 487–566.
[14] Samarov V, Seliverstov D, Froes FHS. Fabrication of near-net-shape cost-effective titanium components by use of prealloyed powders and hot isostatic pressing. In: Titanium powder metallurgy. Elsevier; 2015. p. 313–36. https://doi.org/10.1016/B978-0-12-800054-0.00018-6.
[15] Ageev SV, Girshov VL. Hot isostatic pressing of metal powders. Metallurgist 2015;59(7–8):647–52. https://doi.org/10.1007/s11015-015-0153-y.
[16] Broeckmann C. Hot isostatic pressing of near net shape components – process fundamentals and future challenges. Powder Metall 2013;55(3):176–9. https://doi.org/10.1179/0032589912z.00000000063.
[17] Qadir A, et al. Effect of the oxidization of Si3N4 powder on the microstructural and mechanical properties of hot isostatic pressed silicon nitride. Ceram Int 2018;44(12):14601–9. https://doi.org/10.1016/j.ceramint.2018.05.081.
[18] Vadolia GR, et al. Introduction to isostatic pressing and its optimization." modeling and optimization in manufacturing: toward greener production by integrating computer simulation. https://doi.org/10.1002/9783527825233.ch6; 2021.
[19] Becker L, et al. Validation of the powder metallurgical processing of duplex stainless steels through hot isostatic pressing with integrated heat treatment. Materials 2022;15(18). https://doi.org/10.3390/ma15186224.
[20] MarketsandMarkets. Isostatic pressing market - global forecast to 2028. 2024.
[21] Krautkrämer J, Krautkrämer H. Ultrasonic testing of materials. 4 ed. Springer Science & Business Media; 2013. https://doi.org/10.1007/978-3-662-10680-8.
[22] Cooper AJ, Brayshaw WJ, Sherry AH. Tensile fracture behavior of 316L austenitic stainless steel manufactured by hot isostatic pressing. Metall Mater Trans 2018;49(5):1579–91. https://doi.org/10.1007/s11661-018-4518-2.
[23] Eklund A, Ahlfors M. Heat treatment of PM parts by hot isostatic pressing. Met Powder Rep 2018;73(3):163–9. https://doi.org/10.1016/j.mprp.2018.01.001.
[24] Fleischmann B, et al. Influence of particle size on surface oxide of 316L stainless steel powders for hot isostatic pressing. Materialia 2022;22. https://doi.org/10.1016/j.mtla.2022.101405.
[25] Essa K, et al. An iterative approach of hot isostatic pressing tooling design for net-shape IN718 superalloy parts. Int J Adv Manuf Technol 2015;83(9–12):1835–45. https://doi.org/10.1007/s00170-015-7603-3.
[26] Yuan W, et al. Computer modelling and tooling design for near net shaped components using hot isostatic pressing. J Mater Process Technol 2007;182(1–3):39–49. https://doi.org/10.1016/j.jmatprotec.2006.07.006.
[27] Van Nguyen C, Bezold A, Broeckmann C. Anisotropic shrinkage during hip of encapsulated powder. J Mater Process Technol 2015;226:134–45. https://doi.org/10.1016/j.jmatprotec.2015.06.037.
[28] ElRakayby H, Kim K. Effect of glass container encapsulation on deformation and densification behavior of metal powders during hot isostatic pressing. Int J Material Form 2017;11(4):517–25. https://doi.org/10.1007/s12289-017-1361-8.
[29] Van Nguyen C, Bezold A, Broeckmann C. Final shape prediction of PM HIP components by numerical simulation. In: CFI ceramic forum international; 2015.
[30] Hjorth C-G, Hebeisen JC. Subsea manifolds: an alternate fabrication strategy using HIP PM near net shapes. In: ASME pressure vessels and piping conference; 2005. https://doi.org/10.1115/PVP2005-71156.
[31] Royce R. Europe aims to make pressing a HIP reality. Met Powder Rep 2011;66. https://doi.org/10.1016/S0026-0657(11)70075-3.
[32] Elguezabal B, et al. A multiscale material model for metallic powder compaction during hot isostatic pressing. Powder Technol 2023;425:118599. https://doi.org/10.1016/j.powtec.2023.118599.
[33] Singh S, Ramakrishna S, Singh R. Material issues in additive manufacturing: a review. J Manuf Process 2017;25:185–200. https://doi.org/10.1016/j.jmapro.2016.11.006.
[34] Šuštaršič B, et al. The influence of MoS2 additions on the densification of water-atomized HSS powders. J Mater Process Technol 2006;173(3):291–300. https://doi.org/10.1016/j.jmatprotec.2005.04.122.
[35] Johnson J. Sintering of refractory metals. In: Sintering of advanced materials. Elsevier; 2010. p. 356–88. https://doi.org/10.1533/9781845699949.3.356.
[36] Leonhardt T, Moore N, Hamister M. Spherical rhenium metal powder. 2001.
[37] Kassym K, Perveen A. Atomization processes of metal powders for 3D printing. Mater Today Proc 2020;26:1727–33. https://doi.org/10.1016/j.matpr.2020.02.364.
[38] Vaz R, et al. The influence of the powder characteristics on 316l stainless steel coatings sprayed by cold gas spray. coatings, 11; 2021. p. 168. https://doi.org/10.3390/coatings11020168. 2021, s Note: MDPI stays neutral with regard to jurisdictional claims in published.
[39] Zhang M, Zhang Z, Liu Q. Research advances in close-coupled atomizer flow and atomizing mechanisms. Powder Metall Met Ceram 2023;62(7):400–26. https://doi.org/10.1007/s11106-024-00403-x.
[40] Sun P, et al. Review of the methods for production of spherical Ti and Ti alloy powder. JOM 2017;69(10):1853–60. https://doi.org/10.1007/s11837-017-2513-5.

[41] Azevedo JM, CabreraSerrenho A, Allwood JM. Energy and material efficiency of steel powder metallurgy. Powder Technol 2018;328:329–36. https://doi.org/10.1016/j.powtec.2018.01.009.
[42] Dunkley J. Advances in atomisation techniques for the formation of metal powders. In: Advances in powder metallurgy. Elsevier; 2013. p. 3–18. https://doi.org/10.1533/9780857098900.1.3.
[43] Itiat NE, Ekanem II, Ikpe AE. Prospects of powder metallurgy as the fundamental technique in the production of titanium alloys for the aerospace industries. Biocompounds 2025;2(2):98–115. https://doi.org/10.48313/bic.vi.37.
[44] Muzangaza E. The effects of titanium Ti-6Al-4V powders manufactured using electron beam melting (EBM)-additive manufacturing on metallurgical evaluation. University of Birmingham; 2018. https://files01.core.ac.uk/download/pdf/161936033.pdf.
[45] Chen X, et al. Effect of powder particle size on the fabrication of Ti-6Al-4V using laser metal deposition from elemental powder mixture. https://doi.org/10.17265/2159-5275/2016.07.005; 2016.
[46] Riabov D, et al. Effect of atomization on surface oxide composition in 316L stainless steel powders for additive manufacturing. Surf Interface Anal 2020;52(11):694–706. https://doi.org/10.1002/sia.6846.
[47] Robinson KJ, Thissen H. Selecting the best surface analysis method for your materials/samples. J Vac Sci Technol A 2024;42(4). https://doi.org/10.1116/6.0003576.
[48] Slotwinski JA, et al. Characterization of metal powders used for additive manufacturing. J Res Nat Inst Standards Technol 2014;119:460. https://doi.org/10.6028/jres.119.018.
[49] Guo R, et al. Effect of powder surface state on microstructure and tensile properties of a novel near α-Ti alloy using hot isostatic pressing. Mater Sci Eng, A 2017;706:57–63. https://doi.org/10.1016/j.msea.2017.08.096.
[50] Zhang Q, et al. Effect of humid atmosphere on the microstructure and mechanical properties of a PM Ni-based superalloy: from powders to bulk alloys. Mater Char 2023;202:113019. https://doi.org/10.1016/j.matchar.2023.113019.
[51] Qiu CL, et al. Influence of hot isostatic pressing temperature on microstructure and tensile properties of a nickel-based superalloy powder. Mater Sci Eng, A 2013;564:176–85. https://doi.org/10.1016/j.msea.2012.11.084.
[52] Tan L, et al. Effects of temperature and pressure of hot isostatic pressing on the grain structure of powder metallurgy superalloy. Materials 2018;11(2):328.
[53] Kuo Y-L, Kakehi K. Effect of the prior particle boundary on the microstructure and mechanical properties of hot-isostatic-pressed IN718 alloy. Mater Trans 2017;58(7):1042–8. https://doi.org/10.2320/matertrans.M2017045.
[54] Rao GA, Srinivas M, Sarma D. Effect of thermomechanical working on the microstructure and mechanical properties of hot isostatically pressed superalloy inconel 718. Mater Sci Eng, A 2004;383(2):201–12. https://doi.org/10.1016/j.msea.2004.05.062.
[55] Li P, et al. Effects of ball milling on powder particle boundaries and properties of ODS copper. High Temp Mater Process 2021;40(1):361–9. https://doi.org/10.1515/htmp-2021-0036.
[56] Sun D, et al. Microstructure and high-temperature tensile behavior of superalloy prepared by hot oscillatory pressing. Mater Char 2022;194:112488. https://doi.org/10.1016/j.matchar.2022.112488.
[57] Sun D, et al. Markedly enhancing mechanical properties of powder metallurgy superalloy by hot oscillatory forging. J Mater Res Technol 2024;30:8482–7. https://doi.org/10.1016/j.jmrt.2024.05.219.
[58] Gaikwad S, et al. Mechanical properties and deformation mechanism at elevated temperatures of IN718 superalloy processed by powder forging. Mater Sci Eng, A 2025;924:147803. https://doi.org/10.1016/j.msea.2025.147803.
[59] Qin S, Yan L, Zhang X. Removing prior particle boundaries in a powder superalloy based on the interaction between pulsed electric current and chain-like structure. J Mater Sci Technol 2021;87:95–100. https://doi.org/10.1016/j.jmst.2021.03.003.
[60] Bassini E, et al. Effect of the particle size distribution on physical properties, composition, and quality of gas atomized astroloy powders for HIP application. J Alloys Compd 2022;890. https://doi.org/10.1016/j.jallcom.2021.161631.
[61] Carney CS, et al. Isothermal decomposition kinetics of nickel (II) hydroxide powder. J Alloys Compd 2015;644:968–74. https://doi.org/10.1016/j.jallcom.2015.03.256.
[62] Zhang Q, et al. Effects of composition and particle size on the surface state and degassing behavior of nickel-based superalloy powders. Appl Surf Sci 2021;556:149793. https://doi.org/10.1016/j.apsusc.2021.149793.
[63] Qu Z, et al. Influence of powder particle size on the microstructure of a hot isostatically pressed superalloy. J Mater Res Technol 2022;16:1283–92. https://doi.org/10.1016/j.jmrt.2021.12.081.
[64] MacDonald J, et al. Influence of powder characteristics on the microstructure and mechanical properties of HIPped CM247LC Ni superalloy. Mater Des 2019;174:107796. https://doi.org/10.1016/j.matdes.2019.107796.
[65] Maziarz J, Isaacs J. Techno-economic analysis of PM HIP processing. Powder Metall 2002;45(1):10. https://doi.org/10.1179/pom.2002.45.1.10.
[66] Hjorth C-G. HIP powder metal near-net shapes for demanding environment and applications. J Iron Steel Res Int 2007;14(5):121–5. https://doi.org/10.1016/S1006-706X(08)60064-3.
[67] Zhilin P, et al. The problem of capsule manufacturing for hot isostatic pressing. In: IOP conference series. Materials science and engineering. IOP Publishing; 2020. https://doi.org/10.1088/1757-899X/971/2/022049.
[68] Jasper B, et al. Powder metallurgical tungsten fiber-reinforced tungsten. In: Materials science forum. Trans Tech Publ; 2015. https://doi.org/10.4028/www.scientific.net/MSF.825-826.125.
[69] Kim Y, et al. Fabrication and mechanical properties of powder metallurgy tantalum prepared by hot isostatic pressing. Int J Refract Metals Hard Mater 2015;48:211–6. https://doi.org/10.1016/j.ijrmhm.2014.09.012.
[70] Riehm S, et al. Net-shape components produced by combining additive manufacturing and hot-isostatic pressing. https://dx.doi.org/10.21741/9781644900031-27; 2017.
[71] Larker HT. Hot isostatic pressing of Ceramics–An overview. Hot Isostat Press 1994;93:343–54.
[72] Plucknett K. Hot isostatic pressing of silicon nitride based ceramics. University of Warwick; 1990. https://wrap.warwick.ac.uk/id/eprint/37879/.
[73] Wills RR, McCoy JK. Interface-reaction-controlled kinetics in the hot isostatic pressing of submicrometer alumina powder. J Am Ceram Soc 1985;68(4):C-95–6. https://doi.org/10.1111/j.1151-2916.1985.tb15304.x.
[74] Ltd T. Near net shape powder metallurgy hot isostatic pressing. Available from: https://www.twi-global.com/media-and-events/press-releases/2021/near-net-shape-powder-metallurgy-hot-isostatic-pressing; 2021.
[75] Cai C, et al. Effect of hot isostatic pressing procedure on performance of Ti6Al4V: surface qualities, microstructure and mechanical properties. J Alloys Compd 2016;686:55–63. https://doi.org/10.1016/j.jallcom.2016.05.280.
[76] Bassini E, et al. Net shape HIPping of a Ni-superalloy: a study of the influence of an as-leached surface on mechanical properties. J Mater Process Technol 2019;271:476–87. https://doi.org/10.1016/j.jmatprotec.2019.04.027.
[77] Yang L, et al. Near-net shape hot isostatic pressing: microstructural analysis and hardness evolution at a steel–nickel alloy interface. Adv Mater Interfac 2022;9(11). https://doi.org/10.1002/admi.202101787.
[78] Nagaram AB, et al. Full density powder metallurgical cold work tool steel through nitrogen sintering and capsule-free hot isostatic pressing. Metals 2024;14(8):914. https://doi.org/10.3390/met14080914.
[79] Vattur Sundaram M, et al. Capsule-free hot isostatic pressing of sintered steel to full density using water atomised iron and Cr-alloyed powder consolidated by cold isostatic pressing. Powder Metall 2022;65(2):133–40. https://doi.org/10.1080/00325899.2021.1966876.
[80] Mirz M. A comparative study on different joining techniques for PM-HIP evacuation tubes. https://doi.org/10.59499/WP225370176; 2022.
[81] Riehm S, et al. Tailor-made functional composite components using additive manufacturing and hot isostatic pressing. Powder Metall 2021;64(4):295–307. https://doi.org/10.1080/00325899.2021.1901398.
[82] Geenen K, Röttger A, Theisen W. Corrosion behavior of 316L austenitic steel processed by selective laser melting, hot-isostatic pressing, and casting. Mater Corros 2017;68(7):764–75. https://doi.org/10.1002/maco.201609210.
[83] Liverani E, et al. The effects of hot isostatic pressing (HIP) and solubilization heat treatment on the density, mechanical properties, and microstructure of austenitic stainless steel parts produced by selective laser melting (SLM). Int J Adv Manuf Technol 2020;107:109–22. https://doi.org/10.1007/s00170-020-05072-9.
[84] Irukuvarghula S, et al. Evolution of grain boundary network topology in 316L austenitic stainless steel during powder hot isostatic pressing. Acta Mater 2017;133:269–81. https://doi.org/10.1016/j.actamat.2017.04.068.
[85] Liu G-c, et al. Simulation of pressure effects on hot isostatic pressing of stainless steel powder. J Cent South Univ 2012;19(1):55–62. https://doi.org/10.1007/s11771-012-0972-y.
[86] Hassanin H, et al. Stainless steel with tailored porosity using canister-free hot isostatic pressing for improved osseointegration implants. J Mater Chem B 2017;5(47):9384–94. https://doi.org/10.1039/C7TB02444D.
[87] Kim HS. Densification mechanisms during hot isostatic pressing of stainless steel powder compacts. J Mater Process Technol 2002;123(2):319–22. https://doi.org/10.1016/S0924-0136(02)00104-8.
[88] Essa K, et al. Porosity control in 316L stainless steel using cold and hot isostatic pressing. Mater Des 2018;138:21–9. https://doi.org/10.1016/j.matdes.2017.10.025.
[89] Rao GA, Kumar M. High performance stainless steel via powder metallurgy hot isostatic pressing. Mater Sci Technol 1997;13(12):1027–32. https://doi.org/10.1179/mst.1997.13.12.1027.
[90] Pei Y, et al. Study on the hot deformation characterization of borated stainless steel by hot isostatic pressing. Materials 2021;14(23):7110. https://doi.org/10.3390/ma14237110.
[91] Cooper AJ, et al. A microstructural study on the observed differences in charpy impact behavior between hot isostatically pressed and forged 304L and 316L austenitic stainless steel. Metall Mater Trans 2015;46:5126–38. https://doi.org/10.1007/s11661-015-3140-9.
[92] Cooper AJ, et al. Effect of oxygen content upon the microstructural and mechanical properties of type 316L austenitic stainless steel manufactured by hot isostatic pressing. Metall Mater Trans 2016;47:4467–75. https://doi.org/10.1007/s11661-016-3612-6.
[93] Irvine KJPFB, Gladman T. Grain-refined C-Mn steels. Iron Steel Inst Japan 1967;205(2):161–82.
[94] Cooper AJ, Brayshaw W, Sherry A. Effect of temperature on the fracture toughness of hot isostatically pressed 304L stainless steel. Metall Mater Trans 2018;49:811–6. https://doi.org/10.1007/s11661-018-4466-x.
[95] Hellman P. ASEA-STORA process. Iron Steel 1970;49–52. Special Issue.
[96] Hellman P. As-HIPed APM high speed steels. Met Powder Rep 1992;47(6):25–6. https://doi.org/10.1016/0026-0657(92)91394-Y.
[97] Yao J, et al. Inclusion-controlled high cycle fatigue behavior of a high V alloyed powder metallurgy cold-working tool steel. Mater Sci Eng, A 2011;528(12):4180–6. https://doi.org/10.1016/j.msea.2011.02.016.

[98] Takigawa H, et al. Properties of high-speed steels produced by powder metallurgy. Powder Metall 1981;24(4):196–202. https://doi.org/10.1179/pom.1981.24.4.196.
[99] Furuya K, Jitsukawa S, Saito T. Application of the sinter-HIP method to manufacture Cr–Mo–W–V–Co high-speed steel via powder metallurgy. Materials 2022;15(6):2300. https://doi.org/10.3390/ma15062300.
[100] Mesquita RA, Barbosa CA. High-speed steels produced by conventional casting, spray forming and powder metallurgy. In: Materials science forum. Trans Tech Publ; 2005. https://doi.org/10.4028/www.scientific.net/MSF.498-499.244.
[101] Jung I. Ermüdungsfestigkeit hochlegierter Werkzeugstähle. HTM J Heat Treat Mater 2010;65(5):278–84. https://doi.org/10.3139/105.110074.
[102] Scholl LM, Bezold A, Broeckmann C. Influences of manufacturing-related microstructural variations on fatigue in carbide-rich tool steels. Steel Res Int 2023;94(4):2200578. https://doi.org/10.1002/srin.202200578.
[103] Benito S, et al. Uncovering process-structure relationships associated to the hot isostatic pressing of the high-speed steel PMHS 3-3-4 through novel microstructural characterization methods. Mater Des 2021;208:109925. https://doi.org/10.1016/j.matdes.2021.109925.
[104] Gao L, et al. Study on microstructure and properties between alloy steel and powder steel via hot isostatic pressing diffusion bonding. Mater Today Commun 2024;41:110390. https://doi.org/10.1016/j.mtcomm.2024.110390.
[105] Lindwall G, et al. Experimental and theoretical investigations of hot isostatically pressed–produced stainless steel/high alloy tool steel compound materials. Metall Mater Trans 2011;42:1165–72. https://doi.org/10.1007/s11661-010-0480-3.
[106] Geenen K, et al. Microstructure, mechanical, and tribological properties of M3: 2 high-speed steel processed by selective laser melting, hot-isostatic pressing, and casting. Addit Manuf 2019;28:585–99. https://doi.org/10.1016/j.addma.2019.05.028.
[107] Bayer E, Seilstorfer H. Pulvermetallurgisch durch heißisostatisches Pressen hergestellter Warmarbeitsstahl X 40 CrMoV 5 1. Arch für das Eisenhuttenwes 1984;55(4):169–76. https://doi.org/10.1002/srin.198405330.
[108] Kim K, Jeon Y. Densification behavior and grain growth of tool steel powder under high temperature. Acta Mater 1998;46(16):5745–54. https://doi.org/10.1016/S1359-6454(98)00261-4.
[109] Pagounis E, Talvitie M, Lindroos V. Microstructure and mechanical properties of hot work tool steel matrix composites produced by hot isostatic pressing. Powder Metall 1997;40(1):55–61. https://doi.org/10.1179/pom.1997.40.1.55.
[110] Kumar K, Lawley A, Koczak M. Powder metallurgy T15 tool steel: part I. Characterization of powder and hot isostatically pressed material. Metall Trans A 1991;22:2733–45. https://doi.org/10.1007/BF02851368.
[111] Perevoshchikova N, Hutchinson CR, Wu X. The design of hot-isostatic pressing schemes for Ti–5Al–5Mo–5V–3Cr (Ti-5553). Mater Sci Eng, A 2016;657:371–82. https://doi.org/10.1016/j.msea.2016.01.082.
[112] Cai C, et al. Effect of tooling material on the internal surface quality of Ti6Al4V parts fabricated by hot isostatic pressing. Metall Mater Trans 2017;48:34–8. https://doi.org/10.1007/s11661-016-3796-9.
[113] Zhu L, et al. Effects of microstructure characteristics on the tensile properties and fracture toughness of TA15 alloy fabricated by hot isostatic pressing. Int J Min Met Mater 2023;30(4):697–706. https://doi.org/10.1007/s12613-021-2371-6.
[114] Guang Z, et al. Microstructures and mechanical properties of hot isostatic pressed parts of Ti-6al-4veli alloy spherical powders with three different diameter distributions. Rare Met Mater Eng 2017;46(11):3197–203. https://doi.org/10.1016/S1875-5372(18)30028-6.
[115] Li J, et al. Effect of thermo-hydrogen-treatment on the surface oxide film and the compaction temperature of Ti-47Al-2Cr-2Nb pre-alloyed powders during hot-isostatic-pressing. Int J Hydrogen Energy 2019;44(18):9378–85. https://doi.org/10.1016/j.ijhydene.2019.01.242.
[116] Li W, et al. Enhanced mechanical property with refined microstructure of a novel γ-TiAl/TiB2 metal matrix composite (MMC) processed via hot isostatic press. Mater Des 2018;141:57–66. https://doi.org/10.1016/j.matdes.2017.12.026.
[117] Cai C, et al. A novel near α-Ti alloy prepared by hot isostatic pressing: microstructure evolution mechanism and high temperature tensile properties. Mater Des 2016;106:371–9. https://doi.org/10.1016/j.matdes.2016.05.092.
[118] Xue PJ, et al. Hot isostatic pressing of Ti6Al4V alloys monolithic bladed disks. Appl Mech Mater 2014;496:279–83. https://doi.org/10.4028/www.scientific.net/AMM.496-500.279.
[119] Kim Y, et al. Microstructure and mechanical properties of hot isostatically pressed Ti–6Al–4V alloy. J Alloys Compd 2014;603:207–12. https://doi.org/10.1016/j.jallcom.2014.03.022.
[120] Abena A, Aristizabal M, Essa K. Comprehensive numerical modelling of the hot isostatic pressing of Ti-6Al-4V powder: from filling to consolidation. Adv Powder Technol 2019;30(11):2451–63. https://doi.org/10.1016/j.apt.2019.07.011.
[121] Cai C, et al. A novel hybrid selective laser melting/hot isostatic pressing of near-net shaped Ti-6Al-4V alloy using an in-situ tooling: interfacial microstructure evolution and enhanced mechanical properties. Mater Sci Eng, A 2018;717:95–104. https://doi.org/10.1016/j.msea.2018.01.079.
[122] Mouritz AP. Introduction to aerospace materials. Elsevier; 2012. https://doi.org/10.1533/9780857095152.
[123] Rao GA, Srinivas M, Sarma D. Effect of oxygen content of powder on microstructure and mechanical properties of hot isostatically pressed superalloy inconel 718. Mater Sci Eng, A 2006;435:84–99. https://doi.org/10.1016/j.msea.2006.07.053.
[124] Tian X, et al. Effect of powder size segregation on the mechanical properties of hot isostatic pressing inconel 718 alloys. J Mater Res Technol 2022;21:84–96. https://doi.org/10.1016/j.jmrt.2022.09.009.
[125] Sergi A, Khan RH, Attallah MM. The role of powder atomisation route on the microstructure and mechanical properties of hot isostatically pressed inconel 625. Mater Sci Eng, A 2021;808:140950. https://doi.org/10.1016/j.msea.2021.140950.
[126] Wang JW, et al. Study on direct hot isostatic pressing technology for superalloy inconel 625. Adv Mater Res 2011;189:2935–8. https://doi.org/10.4028/www.scientific.net/AMR.189-193.2935.
[127] Kalahroudi FJ, et al. On the microstructure and high cycle fatigue of near-net shape PM-HIPed inconel 625. Mater Sci Eng, A 2023;886:145671. https://doi.org/10.1016/j.msea.2023.145671.
[128] Sergi A, et al. Development of Ni-base metal matrix composites by powder metallurgy hot isostatic pressing for space applications. Adv Powder Technol 2022;33(2):103411. https://doi.org/10.1016/j.apt.2021.103411.
[129] Chen Y, et al. Comparative study of IN600 superalloy produced by two powder metallurgy technologies: Argon atomizing and plasma rotating electrode process. Vacuum 2018;156:302–9. https://doi.org/10.1016/j.vacuum.2018.07.050.
[130] Chang S-H, et al. Effects of temperature of HIP process on characteristics of inconel 718 superalloy. Int J Cast Metals Res 2006;19(3):175–80. https://doi.org/10.1179/136404606225023399.
[131] Chang SH, et al. Evaluation of HIP pressure on inconel 718 superalloy. Int J Cast Metals Res 2013;19(3):181–7. https://doi.org/10.1179/136404606225023408.
[132] Sreenu B, et al. Microstructure and mechanical behaviour of an advanced powder metallurgy nickel base superalloy processed through hot isostatic pressing route for aerospace applications. Mater Sci Eng, A 2020;797:140254. https://doi.org/10.1016/j.msea.2020.140254.
[133] Yi S, et al. Role of inclusion clusters on fatigue crack initiation in powder metallurgy nickel-based FGH96 superalloy. J Mater Res Technol 2024;33:1286–98. https://doi.org/10.1016/j.jmrt.2024.09.158.
[134] Qiu C, et al. Microstructural development and tensile behavior of a hot isostatically pressed nickel-based superalloy. Mater Sci Eng, A 2020;769:138461. https://doi.org/10.1016/j.msea.2019.138461.
[135] Qiu C, et al. Influence of heat treatment on microstructure and tensile behavior of a hot isostatically pressed nickel-based superalloy. J Alloys Compd 2013;578:454–64. https://doi.org/10.1016/j.jallcom.2013.06.045.
[136] Zeybek Ü, Karaoğlu S. Effects of mechanical alloying on Ni-Rich NiTi shape memory alloys produced by hot isostatic pressing. Russ J Non-Ferrous Metals 2022;63(3):336–43. https://doi.org/10.3103/S1067821222030130.
[137] Wadsworth J, Roberts C, Rennhack E. Creep behaviour of hot isostatically pressed niobium alloy powder compacts. J Mater Sci 1982;17:2539–46. https://doi.org/10.1007/BF00543885.
[138] Desmaison-Brut M, Alexandre N, Desmaison J. Comparison of the oxidation behaviour of two dense hot isostatically pressed tantalum carbide (TaC and Ta2C) materials. J Eur Ceram Soc 1997;17(11):1325–34. https://doi.org/10.1016/S0955-2219(96)00235-X.
[139] Morris RA, et al. Microstructural formations and phase transformation pathways in hot isostatically pressed tantalum carbides. Acta Mater 2012;60(1):139–48. https://doi.org/10.1016/j.actamat.2011.09.036.
[140] Navarrete-Cuadrado J, et al. Hot isostatic pressing of WB4 and WB4-TaB2 based ultrahard materials. Int J Refract Metals Hard Mater 2022;109:105965. https://doi.org/10.1016/j.ijrmhm.2022.105965.
[141] Dias M, et al. Consolidation of W–Ta composites: hot isostatic pressing and spark and pulse plasma sintering. Fusion Eng Des 2015;98:1950–5. https://doi.org/10.1016/j.fusengdes.2015.06.178.
[142] Wang Y, Wang F, Wang Y. Numerical simulation and verification of hot isostatic pressing densification process of W-Cu powder. Mater Res Express 2022;9(7):076503. https://doi.org/10.1088/2053-1591/ac7ea1.
[143] Anwer Z, et al. Microstructure and mechanical properties of hot isostatic pressed tungsten heavy alloy with FeNiCoCrMn high entropy alloy binder. J Mater Res Technol 2023;22:2897–909. https://doi.org/10.1016/j.jmrt.2022.12.078.
[144] Suryanarayanan R, Sastry S, Jerina K. Consolidation of molybdenum disilicide based materials by hot isostatic pressing (HIP): comparison with models. Acta Metall Mater 1994;42(11):3741–50. https://doi.org/10.1016/0956-7151(94)90439-1.
[145] Suryanarayanan R, Sastry S, Jerina K. Mechanical properties of molybdenum disilicide based materials consolidated by hot isostatic pressing (HIP). Acta Metall Mater 1994;42(11):3751–7. https://doi.org/10.1016/0956-7151(94)90440-5.
[146] Wu Z-M, et al. High-dense nanocrystalline W-based alloy prepared by hot isostatic pressing with uniform microstructure, ultrahigh hardness and good thermal stability. Tungsten 2024:1–17. https://doi.org/10.1007/s42864-024-00296-8.
[147] Abdallah A, et al. Effect of applying hot isostatic pressing on the microstructure and mechanical properties of tungsten heavy alloys. In: International conference on aerospace sciences and aviation technology. The Military Technical College; 2017. https://doi.org/10.21608/asat.2017.22790.
[148] Hu B, et al. Densification behavior of tungsten alloy powders during hot isostatic pressing. Mater Today Commun 2022;31:103576. https://doi.org/10.1016/j.mtcomm.2022.103576.
[149] Azcona I, et al. Hot isostatic pressing of ultrafine tungsten carbide-cobalt hardmetals. J Mater Sci 2002;37:4189–95. https://doi.org/10.1023/A:1020048105585.
[150] Bingert SR, Vargas VD, Sheinberg H. Tantalum powder consolidation, modeling and properties. Los Alamos, NM (United States): Los Alamos National Lab.(LANL); 1996. https://doi.org/10.2172/383641.
[151] Boncoeur M, et al. Properties of hot isostatically pressed tantalum. In: Hot isostatic pressing—theory and applications: proceedings of the third international conference Osaka, Japan 10-14 June 1991. Springer; 1991. https://doi.org/10.1007/978-94-011-2900-8.

[152] Leonhardt T, Downs J. Near net shape of powder metallurgy rhenium parts. 2001.
[153] Arzt E, Ashby MF, Easterling KE. Practical applications of hotisostatic pressing diagrams: four case studies. Metall Trans A 1983;14:211–21. https://doi.org/10.1007/BF02651618.
[154] Kissinger R, Nair S, Tien J. Influence of powder particle size distribution and pressure on the kinetics of hot isostatic pressing (HIP) consolidation of P/M superalloy rene 95. Superalloys 1984;1984:285–94. https://doi.org/10.7449/1984/SUPERALLOYS_1984_285_294.
[155] Redouani L, Boudrahem S. Hot isostatic pressing process simulation: application to metal powders. Can J Phys 2012;90(6):573–83. https://doi.org/10.1139/p2012-057.
[156] Redouani L, Boudrahem S. Simulation of the metal and ceramic powders densification process by hot isostatic pressing. Int J Eng Sci Innov Tech 2015;4(3):171–80.
[157] Redouani L, Boudrahem S, Alem S. New hot isostatic pressing (HIP) simulation method with taking into account of the operating cycle ramp. Int J Adv Manuf Technol 2019;102(9):3291–9. https://doi.org/10.1007/s00170-019-03395-w.
[158] Gómez D, Palma R. Phenomenological modeling of Mo in a hot isostatic pressing (HIP) process. Procedia Mater Sci 2015;9:271–8. https://doi.org/10.1016/j.mspro.2015.04.034.
[159] Shima S, Oyane M. Plasticity theory for porous metals. Int J Mech Sci 1976;18(6):285–91. https://doi.org/10.1016/0020-7403(76)90030-8.
[160] Abouaf M, et al. Finite element simulation of hot isostatic pressing of metal powders. Int J Numer Methods Eng 1988;25(1):191–212. https://doi.org/10.1002/nme.1620250116.
[161] ElRakayby H, et al. An investigation of densification behavior of nickel alloy powder during hot isostatic pressing. Adv Powder Technol 2015;26(5):1314–8. https://doi.org/10.1016/j.apt.2015.07.005.
[162] Abondance D, et al. Numerical modelling of near-net-shape hiping of Ti-6 Al-4 V powder 1995;3:2634–40.
[163] Gurson AL. Continuum theory of ductile rupture by void nucleation and growth: part I—yield criteria and flow rules for porous ductile media. https://doi.org/10.1115/1.3443401; 1977.
[164] ElRakayby H, Kim K. Deformation and densification behaviours of nickel-based superalloy during hot isostatic pressing. Powder Metall 2017;60(4):293–300. https://doi.org/10.1080/00325899.2017.1298875.
[165] Fish J, Wagner GJ, Keten S. Mesoscopic and multiscale modelling in materials. Nat Mater 2021;20(6):774–86. https://doi.org/10.1038/s41563-020-00913-0.
[166] Riou A, Olsson S. Trends and applications in PM HIP technology. In: International conference on hot isostatic pressing. Japan: Kobe; 2011.
[167] Flodin A, Andersson M, Miedzinski A. Full density powder metal components through hot isostatic pressing. Met Powder Rep 2017;72(2):107–10. https://doi.org/10.1016/j.mprp.2016.02.057.
[168] Peter WH, et al. Near net shape manufacturing of new, low cost titanium powders for industry. Oak Ridge, TN (United States): Oak Ridge National Lab.(ORNL); 2013.
[169] Horton N, Sheppard R. Benefits of hot isostatic pressure/powdered metal (HIP/PM) and additive manufacturing (AM) to fabricate advanced energy system components. Energy Industries of Ohio, Cleveland, OH (United States) 2016. https://doi.org/10.2172/1417877.
[170] Lerda S, et al. Rapid L-PBF printing of IN718 coupled with HIP-quench: a novel approach to manufacture and heat treatment of a nickel-based alloy. J Mater Res Technol 2024;30:6983–94. https://doi.org/10.1016/j.jmrt.2024.05.128.
[171] Gårdstam J, et al. Latest developments in HIP and high-pressure heat treatment. In: Euro PM2023 proceedings; 2023. https://doi.org/10.59499/ep235763750.
[172] Yang Q-M, et al. Modeling the rheological behavior of a novel hot isostatic pressed powder metallurgy superalloy. Adv Eng Mater 2024;26(4):2300347. https://doi.org/10.1002/adem.202300347.

Jehanzaib Anwar – is a PhD candidate in Materials Science and Technology at Politecnico di Torino (DISAT). His research focuses on advanced manufacturing and post-processing of metallic materials, with emphasis on Hot Isostatic Pressing (HIP) and nickel-based superalloys. He has also co-authored several international publications on alloy reinforcement and life-cycle performance modeling, while also contributing to teaching in materials engineering.
https://scholar.google.com/citations?user=TU7MQKMAAAAJ&hl=en

Emilio Bassini – is an Associate Professor at Politecnico di Torino (DISAT), in Metallurgy. His research primarily focuses on Ni-based superalloys and TiAl alloys, with emphasis on microstructural optimization and improved creep and fatigue resistance. He has been actively involved in major European projects (CleanSky2 HUC, GetReady, NewTeam) and several industrial collaborations (Leonardo, Siemens Energy, GE Avio, Fomas). He has authored more than 50 papers in top international journals (total IF 154.8, h-index 17, over 1200 citations on Scopus), and previously authored papers on JMPT.
https://scholar.google.com/citations?user=mS8FpGwAAAAJ&hl=it

Paolo Fino – is a Full Professor at Politecnico di Torino (DISAT). He is Rector's Advisor for the Mondovì campus and member of the IAM@PoliTo (Integrated Additive Manufacturing) interdepartmental center. His research focuses on metallic additive manufacturing and materials science. He serves on editorial boards (e.g. *Advanced Smart Materials*) and has been awarded recognition such as the "Most Cited Paper 2003–06" by Elsevier-Italy.
https://scholar.google.com/citations?user=E-pFgYgAAAAJ&hl=it

Mariangela Lombardi – is a Full Professor at Politecnico di Torino (DISAT). She is a member of the interdepartmental center IAM@PoliTo (Integrated Additive Manufacturing) and serves as Partnership Agreement Coordinator with GE Avio. Her research focuses on **additive and advanced manufacturing technologies, sustainable manufacturing processes**, and **innovative materials**. She earned a double Ph.D. degree from Politecnico di Torino and INSA Lyon, with a dissertation on cellular ceramics for filtration and biomedical applications.
https://scholar.google.com/citations?user=oBSsL1YAAAAJ&hl=it

Federica Bondioli – is a Full Professor in Materials Science and Technology at Politecnico di Torino (DISAT). She is President of the National Interuniversity Consortium for Materials Science and Technology (INSTM). Her research specializes in developing innovative materials for additive manufacturing, particularly for space, aerospace, and automotive sectors. She has authored more than 210 international publications and leads major national and EU-funded programs (e.g. PISCO, IMPACT, MICS).
https://scholar.google.com/citations?user=-4tn1QsAAAAJ&hl=it

Miren Aristizabal – is a Senior Researcher at CEIT-BRTA, Gipuzkoa (Spain), within the Department of Materials and the Advanced Powder Metallurgy & Laser Manufacturing Group. She holds a B.S. in Chemistry from the University of the Basque Country and a PhD from the University of Navarre. Her over-15 years of research experience span metal powder processing, additive manufacturing, hot isostatic pressing (HIP), and advanced characterization (SEM, FEG-SEM). She has worked in research institutions in Spain, France (CEA), and the UK (University of Birmingham). Her expertise includes materials characterization, sintering, microstructure–property relationships, and process optimization for high-performance metallic systems.
https://scholar.google.com/citations?user=wqMOb4gAAAAJ&hl=en

Íñigo Iturriza Zubillaga – is a Professor Partner at CEIT (Centro de Estudios e Investigaciones Técnicas), collaborating with Tecnun / University of Navarra. He holds the role of Senior Principal Investigator (Investigador Principal Senior). His domain is additive manufacturing, powder metallurgy, HIP/post-HIP heat treatments, microstructure–property relationships in high-temperature alloys, and mechanical testing. His publication record includes ~97 works spanning materials processing, mechanical behavior, and heat treatments. He also takes part in project leadership (e.g. NESMONIC) in industrial/academic collaborations.
https://scholar.google.com/citations?user=fVR-58kAAAAJ&hl=en

Sara Biamino – is a Full Professor at Politecnico di Torino (DISAT), and a member of the interdepartmental IAM@PoliTo center. Her research focuses on additive manufacturing, especially of intermetallics and metallic materials, and advanced materials design and processing. She leads several competitive research projects, including NEUMANN (2022–2027), CNMS Spoke 1 (2022–2025), and TARGET (PRIN). She holds patents in methods for in-situ synthesis and densification of non-oxide ceramics via additive manufacturing technologies.
https://scholar.google.com/citations?user=KI0p6S4AAAAJ&hl=it

Daniele Ugues – is a Full Professor in Metallurgy at Politecnico di Torino (DISAT). He teaches in multiple MSc courses, supervises PhD/MSc students, and coordinates research in additive manufacturing, hot isostatic pressing (HIP), and high-temperature materials. He leads technology transfer and industrial collaborations, and is in charge of the HIP laboratory within IAM@PoliTo. He has strong experience as coordinator and partner in EU and national funded projects.
https://scholar.google.com/citations?user=zDf9wxEAAAAJ&hl=it